AGU PUBLICATIONS

Paleoceanography

RESEARCH ARTICLE
10.1002/2015PA002874

Key Points:
- First complete record of atmospheric $\delta^{13}C$ of CO_2 155 kyr B.P. to present
- Quantification of the effect of the marine biological soft-tissue pump on $[CO_2]$ at the MIS 5-4-3 transitions
- Transfer of isotopically light C to the deep ocean at the onset of MIS 4

Correspondence to:
S. Eggleston,
eggleston@climate.unibe.ch

Citation:
Eggleston, S., J. Schmitt, B. Bereiter, R. Schneider, and H. Fischer (2016), Evolution of the stable carbon isotope composition of atmospheric CO_2 over the last glacial cycle, *Paleoceanography*, *31*, doi:10.1002/2015PA002874.

Received 27 AUG 2015
Accepted 22 FEB 2016
Accepted article online 26 FEB 2016

Evolution of the stable carbon isotope composition of atmospheric CO_2 over the last glacial cycle

S. Eggleston[1,2], J. Schmitt[1,2], B. Bereiter[1,2], R. Schneider[1,2], and H. Fischer[1,2]

[1]Climate and Environmental Physics, Physics Institute, University of Bern, Bern, Switzerland, [2]Oeschger Centre for Climate Change Research, University of Bern, Bern, Switzerland

Abstract We present new $\delta^{13}C$ measurements of atmospheric CO_2 covering the last glacial/interglacial cycle, complementing previous records covering Terminations I and II. Most prominent in the new record is a significant depletion in $\delta^{13}C$(atm) of 0.5‰ occurring during marine isotope stage (MIS) 4, followed by an enrichment of the same magnitude at the beginning of MIS 3. Such a significant excursion in the record is otherwise only observed at glacial terminations, suggesting that similar processes were at play, such as changing sea surface temperatures, changes in marine biological export in the Southern Ocean (SO) due to variations in aeolian iron fluxes, changes in the Atlantic meridional overturning circulation, upwelling of deep water in the SO, and long-term trends in terrestrial carbon storage. Based on previous modeling studies, we propose constraints on some of these processes during specific time intervals. The decrease in $\delta^{13}C$(atm) at the end of MIS 4 starting approximately 64 kyr B.P. was accompanied by increasing $[CO_2]$. This period is also marked by a decrease in aeolian iron flux to the SO, followed by an increase in SO upwelling during Heinrich event 6, indicating that it is likely that a large amount of $\delta^{13}C$-depleted carbon was transferred to the deep oceans previously, i.e., at the onset of MIS 4. Apart from the upwelling event at the end of MIS 4 (and potentially smaller events during Heinrich events in MIS 3), upwelling of deep water in the SO remained reduced until the last glacial termination, whereupon a second pulse of isotopically light carbon was released into the atmosphere.

1. Introduction

Polar ice cores provide a valuable archive of past atmospheric concentrations of climatically important greenhouse gases including CO_2. Ice core research over the past several decades has shown that atmospheric CO_2 concentrations, $[CO_2]$, have varied naturally between approximately 180 and 280 ppm over the past 800 kyr and correlate well with the air temperature over Antarctica [*Jouzel et al.*, 2007; *Lüthi et al.*, 2008]; during glacial periods, $[CO_2]$ was at the lower end of this range, and warmer periods witnessed higher $[CO_2]$. Such a large variation in the atmospheric concentration of this gas indicates that massive shifts of carbon storage between the main reservoirs—atmosphere, terrestrial biosphere, oceans, and sediments—must have occurred on glacial/interglacial timescales.

Atmospheric $[CO_2]$ has been found to vary naturally on millennial timescales as well; it has been hypothesized that such variations are controlled largely by processes occurring in the Southern Ocean (SO) [*Sigman and Boyle*, 2000; *Ahn and Brook*, 2008; *Bereiter et al.*, 2012], including carbon uptake and export by the marine biological soft-tissue pump, reduced subsurface vertical mixing, and increased surface stratification in the SO during glacial times, as well as release through upwelling events documented in the marine sediment record [*Anderson et al.*, 2009; 2014, *Jaccard et al.*, 2013; *Gottschalk et al.*, 2015]. Antarctic ice core and SO marine records are, however, also largely influenced by the Northern Hemisphere through teleconnections including the bipolar seesaw [e.g., *Stocker*, 1998; *Broecker*, 1998; *Stocker and Johnsen*, 2003]: this describes the phenomenon of a reduction of the Atlantic meridional overturning circulation (AMOC) leading to rapid cooling in the Northern Hemisphere but slow warming in the SO. In particular, cold conditions during stadials between Dansgaard-Oeschger (DO) events during the last glacial period correspond to periods of warming in Antarctica [*EPICA Community Members*, 2006]; the longest of these periods are also recorded in the CO_2 record as a rise in $[CO_2]$ [*Bereiter et al.*, 2012; *Ahn et al.*, 2014]. Heinrich events, defined as periods of significant amounts of ice-rafted debris in North Atlantic sediment cores [e.g., *Hemming*, 2004], have also been linked to significant cooling in the Northern Hemisphere, weakening of the AMOC, and significant southward shifts in the

intertropical convergence zone, thus with important implications for [CO_2] [e.g., *Marcott et al.*, 2011; *Barker et al.*, 2015].

Each of the processes by which carbon is transferred from one reservoir to another causes fractionation of the stable carbon isotope to some degree. Thus, measurements of δ^{13}C(atm) can be very useful in understanding both longer- and shorter-term changes in the global carbon cycle. Thus motivated, previous studies reconstructing δ^{13}C(atm) [e.g., *Lourantou et al.*, 2010a, 2010b; *Schmitt et al.*, 2012; *Schneider et al.*, 2013] have made use of this fact to constrain the most important processes involved in the increase of [CO_2] documented at glacial terminations. These studies, complemented by modeling studies [e.g., *Köhler et al.*, 2010; *Menviel et al.*, 2012], have indicated that the most important processes governing [CO_2] at these transitions are (i) increased upwelling in the SO, (ii) warming of the sea surface, (iii) decreased biological export from the surface ocean to depths most likely due to waning of aeolian iron fertilization in the SO, (iv) increase of the formation of North Atlantic Deep Water (NADW), (v) growth of the terrestrial biosphere, and, (vi) on longer timescales, carbonate compensation. These processes partly compensate each other; while warming of the sea surface leads to an increase in both [CO_2] (reduced solubility) and δ^{13}C(atm) (reduced fractionation at the air-sea interface), sea level rise and melting of sea ice have the opposite effects. Similarly, increased upwelling of ^{13}C-depleted and CO_2-rich water in the SO, decreased efficiency of the marine biological soft-tissue pump tied to Fe limitation, as well as increased formation of NADW lead to an increase in [CO_2] but a decrease in δ^{13}C(atm) [*Köhler et al.*, 2010]. In contrast, growth of the terrestrial biosphere (e.g., uptake of isotopically light CO_2) reduces [CO_2] and increases δ^{13}C(atm). Moreover, the net change in δ^{13}C(atm) due to changes in the efficiency of the SO soft-tissue pump may be caused by several processes, which per se cannot be discerned from δ^{13}C(atm) alone, such as changes in iron fertilization, vertical nutrient supply to the SO surface waters by upwelling, or an enhanced stratification of the SO surface ocean. Thus, while it is impossible to disentangle the magnitudes of the impacts of each of these processes on [CO_2] based solely on the stable carbon isotope data, coupled with other proxy records, this provides an important constraint on the system. It has been suggested that the same processes could be used to explain the evolution of [CO_2] and δ^{13}C(atm) during Terminations I and II, though the relative magnitudes and timing of the various processes must have differed [*Schneider et al.*, 2013]. Overall, the results indicate that the SO plays a major role in determining both [CO_2] and δ^{13}C(atm), as previously hypothesized [e.g., *Sigman and Boyle*, 2000; *François et al.*, 1997].

Due to the lack of a complete δ^{13}C(atm) record connecting the various data sets, unanswered questions remained. Most importantly, the penultimate glacial maximum (PGM) was found to be 0.4‰ isotopically lighter in δ^{13}C(atm) than the Last Glacial Maximum (LGM), and the penultimate warm period (marine isotope stage (MIS) 5e) was also more negative in δ^{13}C(atm) by a similar amount. This is a surprisingly large difference, on the order of the changes in δ^{13}C(atm) observed during glacial terminations. Furthermore, it has been hypothesized that a pool of "old" and isotopically light carbon was present at the LGM in the deep oceans, likely connected to an expansion of less well-ventilated Antarctic Bottom Water (AABW) [*Skinner et al.*, 2010]. The release of carbon from this pool into the atmospheric reservoir due to increased upwelling in the SO led to a drop in δ^{13}C(atm) at Termination I [*Anderson et al.*, 2009; *Schmitt et al.*, 2012]. This begs the question as to when over the course of the glacial the transfer of isotopically light carbon from the atmosphere to the deep ocean occurred.

Here we present the first record of δ^{13}C(atm) over the entire last glacial period (Figure 1). Combined with the records published by *Elsig et al.* [2009], *Schmitt et al.* [2012], and *Schneider et al.* [2013], this constitutes the first complete data set over the last 155 kyr, thus elucidating some of the remaining questions regarding changes in the global carbon cycle, both on glacial/interglacial as well as millennial timescales. Our data indicate that the process of carbon transfer to the deep ocean had occurred at or before the MIS 5-4 transition, as proposed by *Hain et al.* [2010] and further discussed by *Bereiter et al.* [2012], *Adkins* [2013], and *Jaccard et al.* [2016].

2. Methods and Data Quality

Due to its relatively high quality of ice over the period of interest, the Talos Dome deep ice core (72°49'S, 159°11'E, length of core: 1620 m, dated to a maximum age of 150 kyr B.P.) was selected as the primary core for this study. To verify the robustness of the results, samples from the deep ice cores European Project for Ice Coring in Antarctica (EPICA) Dome C (EDC; 75°06'S, 123°24'E, length of core: 3270.2 m, dated to a maximum age of 800 kyr B.P.) and EPICA Dronning Maud Land (EDML; 75°00'S, 00°04'E, length of core: 2774 m,

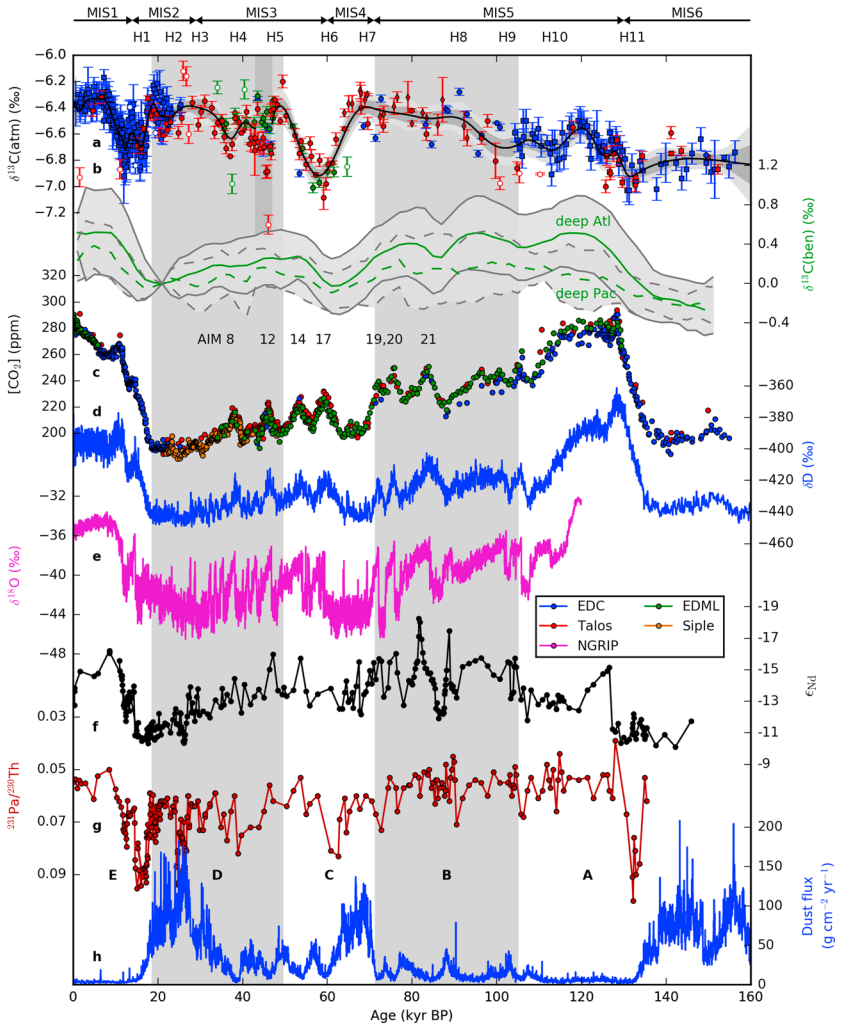

Figure 1. (a) New δ^{13}C(atm) record from 155 kyr B.P. to the present. Outliers, as determined by a bootstrapping method, are shown as open symbols (circles: this study; squares, 25–0 kyr B.P.: *Schmitt et al.* [2012]; squares, 156–104 kyr B.P.: *Schneider et al.* [2013]; diamonds: *Schneider* [2011]). An MCA cubic spline is shown with 1σ and 2σ error bars. In the period 47–43 kyr B.P., there is disagreement between results from EPICA Dronning Maud Land (EDML) and Talos Dome ice; accordingly, no spline is plotted. (b) δ^{13}C(ben) represents deep ocean (2500–5000 m) averages from benthic foraminfera in the Atlantic and Pacific basins, where the value for each species is given relative to its value at the LGM (21 kyr B.P.) (*Oliver et al.* [2010], age scale as published). (c) The [CO_2] record is a compilation from four Antarctic ice cores, showing the natural variability in [CO_2] over the last glacial cycle using new and published data [*Monnin et al.*, 2001; 2004; *Lourantou et al.*, 2010a, 2010b; *Schmitt et al.*, 2012; *Schneider et al.*, 2013; *Siegenthaler et al.*, 2005; *Bereiter et al.*, 2012; *Lüthi et al.*, 2010; *Ahn et al.*, 2014]. (d) δD(H_2O) from EPICA Dome C (EDC) is a proxy for Antarctic temperature, with Antarctic Isotope Maxima indicating warm periods in the Southern Hemisphere [*Jouzel et al.*, 2007]. (e) δ^{18}O(H_2O) from North Greenland Ice Core Project (NGRIP) correlates with Greenland temperature, showing 21 abrupt warming (DO) events since the last interglacial period [*NGRIP Community Members*, 2004]. (f) ϵ_{Nd} [*Böhm et al.*, 2014; *Roberts et al.*, 2010] and (g) ^{231}Pa/^{230}Th [*Böhm et al.*, 2014; *Lippold et al.*, 2009; *McManus et al.*, 2004] from the Bermuda Rise on the timescale as published by *Böhm et al.* [2014]. (h) The EDC dust flux record shows that the three most prominent peaks in Fe fertilization occurred during MIS 6, 4, and 2 [*Lambert et al.*, 2012]. Note that in all figures, all ice core records from EDC, EDML, Talos Dome, and NGRIP have been plotted on the modified AICC2012 age scale [*Bazin et al.*, 2013; *Veres et al.*, 2013, see text].

dated to a maximum age of 140 kyr B.P.) were also measured at specific time intervals to check for inter-core agreement. The Antarctic Ice Core Chronology 2012 (AICC2012) was used for dating the three cores [*Bazin et al.*, 2013; *Veres et al.*, 2013]. However, as shown by *Baumgartner et al.* [2014], the methane records for the cores used in AICC2012 do not match to the required degree over the entire age scale. Thus, for the period 48.5–40 kyr B.P., where all three cores were more intensively measured, slight adjustments to the EDC and EDML AICC2012 timescales were made by matching the CH_4 records from EDC and EDML to the Talos

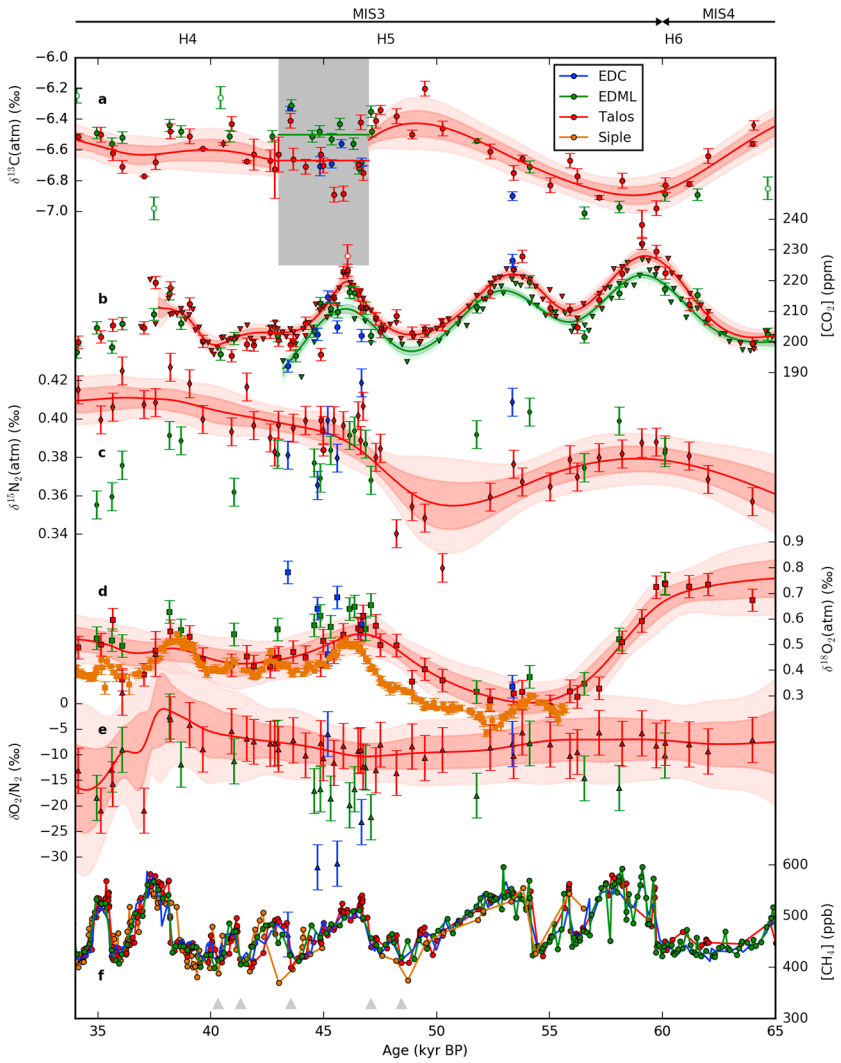

Figure 2. Comparison of data from multiple ice cores and multiple laboratories for the time interval 65–34 kyr B.P. (a) An analytical difference is seen in δ^{13}C(atm) in Talos Dome and EDML between 47 and 43 kyr B.P.; the mean value from each ice core over this period is plotted as a horizontal line. (b) The same ice cores show a small offset in [CO_2] in the interval 62–42 kyr B.P. (circles: this study; triangles: *Bereiter et al.* [2012]). (c) Measured $\delta^{15}N_2$ shows relatively little variability over this period, demonstrating that the firn column in neither ice core changed significantly. (d) Atmospheric $\delta^{18}O_2$ data from this study agree well with those from (*Severinghaus et al.* [2009], age scale as published). All records have been corrected for gravitational fractionation and those from Siple Dome additionally for gas loss. (e) $\delta O_2/N_2$ from EDML, EDC, and Talos Dome indicative of gas loss. (f) The CH_4 records from EDC, EDML, Talos Dome, and Siple Dome match relatively well over this interval, demonstrating the good agreement of the age scales (gray triangles denote tie points for adjusting the EDC, EDML, and Talos Dome age scales), although slight discrepancies may be traced to the fact that the Siple Dome age scale was created by matching the methane record to that of Greenland Ice Sheet Project 2 (GISP2).

Dome record. Five troughs in the record were selected as tiepoints and the offsets to the existing AICC2012 chronologies were then linearly interpolated between the tiepoints. These adjustments lead to differences with the AICC2012 chronologies of no more than 370 years. The good agreement of the methane records in the EDML and Talos Dome ice cores after this adjustment is shown in Figure 2.

For all samples, gas was extracted from the ice using the sublimation device described by *Schmitt et al.* [2011] with one minor but vital adaptation: recollection of the bulk air to measure $\delta^{15}N_2$ in order to remove the gravitational component from the firn and thus derive δ^{13}C(atm) from the measured δ^{13}C in the ice core sample. After collecting CO_2 and N_2O on a stainless steel trap immersed in liquid nitrogen, the bulk air was collected on a removable molecular sieve 5A trap at liquid nitrogen temperature. The bulk gases were released by heating the molecular sieve and analyzed for stable isotope and molecular ratios of the major atmospheric

components ($\delta^{15}N_2$, $\delta^{18}O_2$, $\delta^{40}Ar/^{36}Ar$, $\delta O_2/N_2$, and $\delta Ar/N_2$) using a Thermo Scientific Delta V Plus isotope ratio mass spectrometer (IRMS) in dual-inlet mode. When running sublimation system standards (reference air passed over gas-free ice during the sublimation step, subsequently freezing out CO_2 and N_2O as in the samples), the resulting $\delta^{15}N$ values show a consistent offset from zero of 0.014 to 0.026‰ (range given for the four individual sample fingers) with a standard deviation of 0.008‰ (maximum for all sample fingers). This small offset was thus subtracted from the samples for each of the molecular sieve sample fingers. The result for $\delta^{15}N$ was then used directly as the correction for $\delta^{13}C$ to account for gravitational fractionation in the firn column. This correction is on the order of −0.4‰ and is thus much larger than the offset of the standard air. Based on the pooled standard deviation of replicate samples, the precision of the $\delta^{15}N$ measurement was 0.007‰. In the few cases where $\delta^{15}N$ could not be measured at a certain depth, the interpolated value between neighboring samples was used. As the variations in $\delta^{15}N$ due to gravitational enrichment are only about one-tenth of that of $\delta^{13}C$, the additional error introduced by this approximation is negligible compared to the experimental errors of the $\delta^{13}C$ measurements, which are between 0.05 and 0.1‰.

2.1. Data Quality: Outliers

Two types of outliers have been identified and removed from the data set presented here. If a problem arose during the extraction or IRMS measurement, the resulting values for $\delta^{13}C(atm)$ and $[CO_2]$ were eliminated from the data set. Such issues included leaks in the system detected by unusually high pressure readings, as well as sample contamination, most often caused by ice core drilling fluid. This was encountered primarily in the brittle ice zone of each ice core where the core quality suffers, and cracks allow the drilling fluid to penetrate into the ice sample. For EDML, Talos Dome, and EDC, the brittle ice zone roughly covers the time periods 23–7, 34–11, and 81–24 kyr B.P., respectively [*Neff*, 2014, and references therein]. For all three cores, the densifier in the drilling fluid was Freon141b, which produces a fragment in the mass spectrometer source at m/z = 45, thus an isobar of $^{13}CO_2$ and $CO^{17}O$. Despite gas separation by means of a gas chromatograph, contamination by drilling fluid produced several peaks in the chromatograph separated in time, and samples were thus clearly identifiable in the resulting chromatogram. As a result, however, the sample peaks following a contaminated sample were also eliminated from the final results due to interference in the signal. We cannot exclude the possibility that samples contaminated by very little drilling fluid may fall under these detection limits; this could be a source of the scatter in the $\delta^{13}C(atm)$ data within the brittle ice zones of the respective cores.

The second type of outlier was statistical in nature. To identify such outliers, a Monte Carlo bootstrapping method was employed. For each point, a Monte Carlo cubic spline Average (MCA) was constructed using only all other points in the data set; this method is described in more detail by *Schmitt et al.* [2012]. If the point lay outside of the sum of twice the standard deviation of the spline and twice the standard deviation of the point itself, it was identified as a statistical outlier. Outliers of this type are depicted in Figure 1 as open circles. Of the 229 individual new samples measured in this study at 155 different depths, 60 fell into the first category of outliers; of the remaining 133 different depths sampled, 16 data points were identified as statistical outliers. We thus contribute new $\delta^{13}C(atm)$ values at 117 new time steps to the preexisting database from *Elsig et al.* [2009], *Schmitt et al.* [2012], and *Schneider et al.* [2013].

2.2. Offsets Between Records

Published and unpublished $[CO_2]$ data from Talos Dome and EDML over the period 127–43 kyr B.P. measured at the University of Bern using the cracker extraction system (Talos Dome 68–43 kyr B.P., EDML 113–43 kyr B.P. [*Bereiter et al.*, 2012]; Talos Dome 127–70 kyr B.P., EDML 127–99 kyr B.P. this study) allow us to compare the two ice cores as well as the two methods in the period of overlap with the present study (see Figure 2). Over the most recent part of this period (62–43 kyr B.P.), Talos Dome shows $[CO_2]$ on average 4.7 ppm higher than those measured at EDML [*Bereiter et al.*, 2012]. For older ages, the difference in the two cores is negligible as reported by *Bereiter et al.* [2012]. The stable carbon isotope data show an offset between the cores in the time interval 47–43 kyr B.P. (discussed below), but between 62 and 47 kyr B.P., there is no detectable difference.

For the Talos Dome ice core during the period 62–47 kyr B.P., in situ production of CO_2 from organic precursor material is unlikely to explain the 4.7 ppm offset, because we would expect 0.2–0.4‰ lower $\delta^{13}C$ values (assuming a source signature of approximately −20‰), which is clearly not the case. In the case that the in situ production were from terrestrial carbonate, we would expect 0.15‰ heavier values (source signature around 0‰). Due to the low resolution of the EDML data in this interval, we cannot rule out this possibility; however, based on the available data, this theory does not appear to be in line with our measurements.

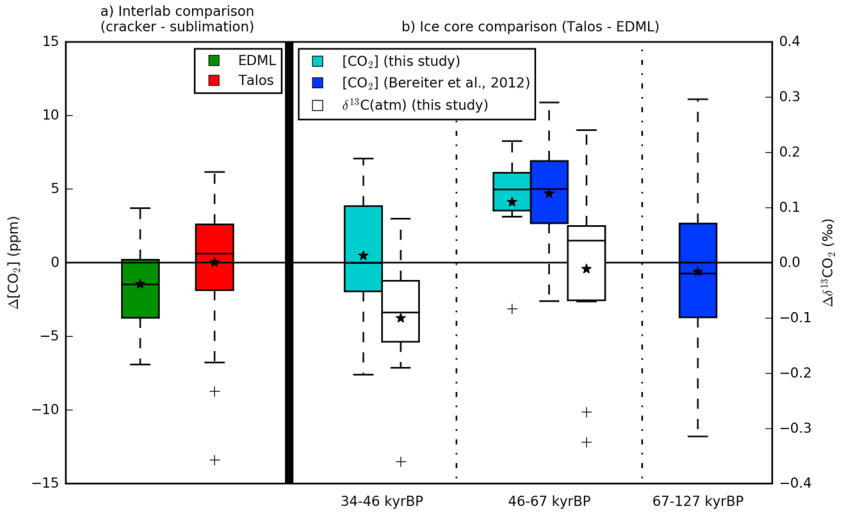

Figure 3. Box plot depicting the agreement and offsets observed in $\delta^{13}C(atm)$ and $[CO_2]$ in this study and *Bereiter et al.* [2012] from Talos Dome and EDML; indicated are means (stars), medians (horizontal bars), and outliers outside of 150% of the interquartile range (plus signs). For each sublimation system measurement, the cracker system measurement nearest in time but not more than 1 kyr away was taken for comparison; similarly for EDML and Talos Dome measurements. (a) $[CO_2]$ data from EDML agree well between the two methods; similarly for data from Talos Dome. (b) Offsets between the cores are seen both in the concentration as well as the isotope data; however, these offsets appear to be unrelated, as the $[CO_2]$ data disagree between 67 and 46 kyr B.P., while the isotope data only show an offset later (46–34 kyr B.P.).

To explain offsets between different $[CO_2]$ ice core records measured with mechanical extraction devices with less than 100% extraction efficiency, *Bereiter et al.* [2012] hypothesized a CO_2 fractionation of clathrates relative to air bubbles in the Bubble-Clathrate Transition Zone (BCTZ). This could lead to different $[CO_2]$ in clathrates of different sizes, together with a slow reequilibration of $[CO_2]$ below the BCTZ by diffusion through the ice between individual clathrates, which may not be complete in EDML in the age range of 62–42 kyr B.P. If the mechanical dry extraction method results in preferential extraction of gas from larger clathrates and bubbles, this reasoning could explain the $[CO_2]$ offset measured by *Bereiter et al.* [2009, 2012]. However, this would also imply that the sublimation method used in this study, with 100% extraction efficiency independent of the physical structure of the ice, should not show a concentration offset, contrary to what is observed. A nearest-neighbor test demonstrates no significant offset between the Talos Dome data measured in this study compared to those presented by *Bereiter et al.* [2009, 2012]; the same holds true for the corresponding EDML data. Accordingly, the offset between the two cores as discussed by Bereiter and colleagues is also documented in the new data presented here using the sublimation method (see Figure 3).

Postcoring gas loss may be an alternative explanation. This has been shown to affect O_2 and potentially N_2 but not CO_2, due to the lower permeation constants of N_2 and CO_2 in ice compared to that of O_2 [*Bereiter et al.*, 2009; *Ikeda-Fukazawa et al.*, 2005] and, in the BCTZ, because of the larger molecular diameter of CO_2 [*Craig et al.*, 1988]. Lower $\delta O_2/N_2$ values in EDML compared to Talos Dome indicate a significant loss of O_2 relative to N_2 in EDML (Figure 2). In the case that only O_2 is lost, this would lead to an increase in $[CO_2]$ in EDML relative to Talos Dome of about 0.4 ppm, contrary to what is observed. In the case that both O_2 and N_2 are lost in EDML after coring, a much stronger change could be expected; again, however, this would lead to higher CO_2 mixing ratios measured at EDML if the gas loss occurred in EDML ice. Alternatively, a higher O_2 and N_2 gas loss in Talos Dome could explain the offset, as this would lead to higher CO_2 mixing ratios in Talos Dome ice; however, to account for the observed $[CO_2]$ offset, at least a loss of 2.7% of total air content would be required in Talos Dome, which is not observed (O. Eicher, unpublished data, 2016). Finally, contamination of the enclosed ancient air with recent air after coring can be excluded because of the good agreement of $\delta^{13}C$ during the period in question. For the moment we cannot explain the 4 ppm $[CO_2]$ offset in the time interval 62–47 kyr B.P.; however, we acknowledge that the number and precision of the new sublimation data may not yet be sufficient to resolve the puzzle.

In contrast to 62–47 kyr B.P., the period 47–43 kyr B.P. (marked in gray in Figure 2) shows a significant difference of 0.17‰ in $\delta^{13}C$ measured on the Talos Dome and EDML ice cores, with the $\delta^{13}C$ values of EDML being higher than Talos Dome. This was verified statistically by using a modified Student *t* test of the detrended data over this interval, which indicates that the $\delta^{13}C(atm)$ offset between Talos Dome and EDML is statistically significant within the 95% confidence level ($p < 0.05$). In the time interval 43–38 kyr B.P., four of the EDML data points agree well with the Talos Dome data while one is elevated by 0.2‰. Based on this limited number of samples, it is not possible to determine whether the EDML and Talos Dome data are different in this interval as well; however, in the time interval 47–43 kyr B.P., the difference is significant. In the following we concentrate on the latter.

The data in the time interval 47–43 kyr B.P. of both cores were measured during the same measurement campaign in the same laboratory, by the same user and with the same system; it is thus unlikely that the observed difference is due to a methodological or standardization problem. Synchronization problems have also been eliminated as a source of error by comparing the CH_4 records measured on these two ice cores (Figure 2). The sublimation technique used in this study results in 100% gas extraction regardless of the relative amounts of gas enclosed in bubbles and clathrates, so changes in the physical composition of the ice due to, e.g., differing storage times and relaxation of the ice should not be observed in these measurements. Thus, it appears likely that the offset in Talos Dome and EDML in this time interval is due to a real difference in $\delta^{13}C$ values of the gas in the ice itself, though this cannot reflect local differences in $\delta^{13}C(atm)$, as over the distance between EDML and Talos Dome, no spatial gradients in $[CO_2]$ or in $\delta^{13}C(atm)$ are to be expected.

From our $\delta^{15}N_2$ measurements (see Figure 2), it is also clear that no drastic change occurred in the depth of the firn column at this point in time associated with possible changes in site temperature or accumulation rate, precluding firn column fractionation effects as a possible explanation for the differences in $[CO_2]$ and $\delta^{13}C$ reported here. The $\delta^{15}N$ signals both in EDML and Talos Dome are rather constant during this period in comparison to the observed $\delta^{13}C$ offset.

Note that Talos Dome $[CO_2]$ is about 6 ppm higher than EDML during the CO_2 peak at 46 kyr. Applying a simple mass balance calculation for this point in time ($C_{obs} = C_{atm} + C_{source}$; $\delta_{obs} \cdot C_{obs} = \delta_{atm} \cdot C_{atm} + \delta_{source} \cdot C_{source}$), we can estimate the isotopic signature of the extra CO_2 in the Talos Dome ice core that could lead to the observed values. With a difference in $[CO_2]$ of 6 ppm and $\delta^{13}C$ approximately −6.5‰ and −6.8‰ at the peak maximum in EDML and Talos Dome, respectively, this approach would indicate a source signature of −17.5‰, hinting at the possibility of potential in situ production of CO_2 from organic material in the Talos Dome ice core at these depths. This is similar to what [*Schneider*, 2011] found when comparing EDML and EDC (128–125 kyr B.P.), where the mean source signature of in situ produced CO_2 in the EDML core was −17.4‰. However, chemically and climatologically, the ice in the time interval 47–43 kyr B.P. is not expected to differ from that in the time interval 62–47 kyr B.P. [*Schüpbach et al.*, 2013], where no $\delta^{13}C$ offset is observed.

Thus, although there is indication in our extended data set that certain time intervals show differences in $\delta^{13}C(atm)$ between cores, these are only sometimes accompanied by differences in $[CO_2]$ and thus cannot be explained solely by in situ production of CO_2. Note as well that there is no evidence for EDML representing more accurate values compared to Talos Dome, but there are very few known processes that can occur within the ice that lead to lower $[CO_2]$ [e.g., *Tschumi and Stauffer*, 2000]; hence, it appears more likely that there is a small amount of CO_2 production in Talos Dome in this interval rather than CO_2 consumption in EDML.

As mentioned above, several samples in the brittle ice zone were found to be contaminated with drilling fluid, thus precluding accurate measurement of $\delta^{13}C(atm)$ on these samples. Furthermore, it is possible that samples containing very little drilling fluid would not be detected by the method outlined above, resulting in an anomalously high value for $\delta^{13}C$ with a nondetectable impact on $[CO_2]$; this would thus be an explanation of the observed isotopic offset if the EDML samples showed evidence of contamination. However, we find this scenario highly unlikely for two reasons. First, this type of contamination has been observed to cause scatter in the data; in samples identified with contamination, the $\delta^{13}C(atm)$ offset is not constant due to differing amounts of drilling fluid in the samples. Second, the samples in question are from 200–400 m below the brittle zone in EDML. Unless the core were of particularly poor quality in this region (1400–1500 m), we have no reason to believe that drilling fluid has penetrated into the ice.

Another mechanism that could account for a difference in both the concentration and isotopic signals of CO_2 is a variation in the bubble enclosure characteristics at this point in time. If the age distribution were much

broader in EDML due to exceptionally low accumulation rates, the amplitudes of both $\delta^{13}C$ and [CO_2] would be dampened, similar to what is seen in this period. However, although it is predicted that the accumulation rate at EDML was reduced with respect to Talos Dome during this period, this reduction is assumed to be at most 25% (0.033 versus 0.045 m water equivalent yr^{-1} at EDML and Talos Dome, respectively) [*Veres et al.*, 2013]. Moreover, such an anomalous dampening would be expected in other gas records as well, but as shown in Figure 2, dampening of the [CH_4] signal is not observed [*Schilt et al.*, 2010; *Buiron et al.*, 2011; *Stenni et al.*, 2011].

In summary, there is good agreement among the $\delta^{13}C$(atm) measurements performed in this study from the three cores except for the time interval 47–43 kyr B.P. We have no straightforward explanation for this discrepancy and cannot determine which of the two records, Talos Dome or EDML, provides the true atmospheric $\delta^{13}C$ signal in this time interval. We accordingly refrain from interpreting the carbon isotopic change in detail during this short interval.

3. Results

Our new record shows a gradual enrichment of $\delta^{13}C$(atm) throughout MIS 5 from the PGM value of −6.8‰ until 68 kyr B.P., at which point it has reached the LGM value of −6.4‰ (Figure 1). Most noteworthy, the $\delta^{13}C$(atm) signal shows no significant change simultaneous with the drop in [CO_2] at the MIS 5-4 transition (circa 70 kyr B.P.); this signal is also not synchronous with net global changes in $\delta^{13}C(CaCO_3)$ in benthic foraminifera, $\delta^{13}C$(ben). A significant drop in $\delta^{13}C$(atm) of approximately 0.5‰, which is on the order of the changes at Termination I (though over a somewhat longer time interval), begins only at around 64 kyr B.P. A subsequent equally strong rise beginning at the MIS 4-3 transition is observed. Once the LGM level has been reached again around 48 kyr B.P. (Heinrich event 5), the scatter in the data in combination with the low resolution renders a detailed millennial-scale analysis difficult. However, there appear to be small declines in $\delta^{13}C$(atm) on the order of 0.1–0.2‰ following Heinrich events 5, 4, and 2. Each of these local minima is followed by a gradual enrichment of about the same order of magnitude. Note that we cannot rule out the possibility of a similar pattern occurring in the data following Heinrich event 3; the data resolution in this time interval precludes any definitive statement regarding this trend.

4. Discussion

To facilitate the discussion of these results, the record between 155 kyr B.P. and present has been divided into five intervals, A–E, as shown in Figure 1; interval C has been further subdivided into seven subintervals. As mentioned above, intervals A and E (Terminations II and I) have previously been published and discussed by *Schneider et al.* [2013] and *Schmitt et al.* [2012]. Accordingly, the focus of this paper is on the time interval of the progressing glaciation from about 120 kyr B.P. to 20 kyr B.P., which connects the previously existing time series and allows for the analysis of the evolution of the global carbon cycle from MIS 5 to MIS 2 (intervals B–D). Throughout the following discussion, we refer to Figure 4 as an indication of the signal expected from various processes in CO_2-$\delta^{13}C$(atm) space [*Köhler et al.*, 2010].

4.1. Carbon Cycle Changes During MIS 5

As mentioned above, the last interglacial (around 120 kyr B.P., also known as MIS 5e) was characterized by about 0.4‰ lower $\delta^{13}C$(atm) values than the Holocene, an offset also seen when comparing the PGM and LGM. Interval B (105–71.4 kyr B.P., or MIS 5d-a) directly following MIS 5e is characterized by an overall increase in $\delta^{13}C$(atm) of 0.2–0.3‰, with $\delta^{13}C$(atm) reaching the MIS 3 and LGM levels for the first time early in MIS 4. Accordingly, Interval B can be regarded as the time period where the enigmatic $\delta^{13}C$(atm) shift between the PGM and LGM and MIS 5e and the Holocene occurs. The largest increase in $\delta^{13}C$(atm) within this interval occurs between 100 and 90 kyr B.P.; however, the resolution of our record does not allow us to pinpoint the time of the $\delta^{13}C$(atm) increase exactly. Interval B is also characterized by only a subtle linear trend in [CO_2] over its entire duration, which, however, is superimposed by significant fluctuations in [CO_2] on the order of 20 ppm synchronous to the Antarctic Isotope Maxima (AIM) seen in Antarctic ice core temperature proxy records [*Bereiter et al.*, 2012; *Ahn and Brook*, 2008; *EPICA Community Members*, 2006].

Several processes could be potentially connected to the carbon cycle changes during this interval: increase in marine biological export in the SO from the surface to depths; weakening of the AMOC over this period, corresponding to enhanced storage of $\delta^{13}C$-depleted carbon in the deep ocean [*Köhler et al.*, 2010]; increase in land carbon stocks, e.g., in Asian peatlands or permafrost at higher latitudes, overcompensating the loss

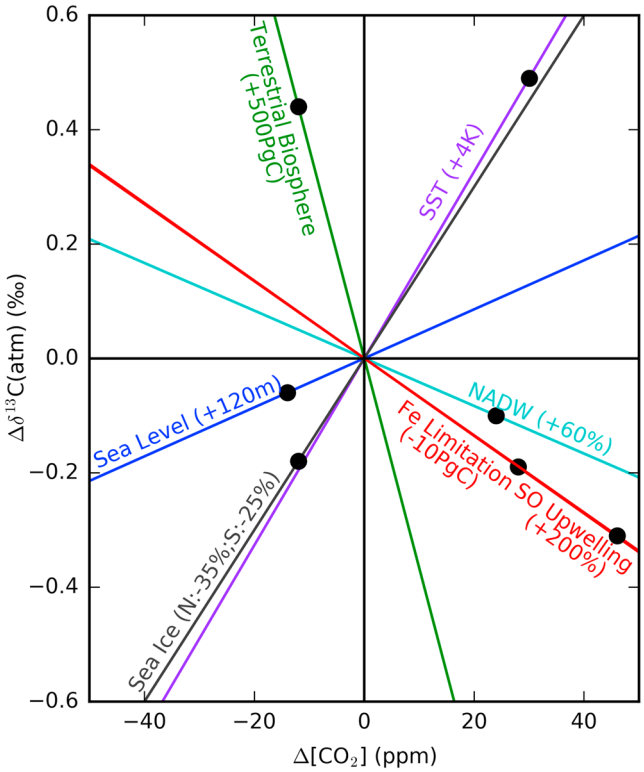

Figure 4. Effects of various processes on $[CO_2]$ and $\delta^{13}C$(atm); the changes of the forcing parameters with respect to modeled LGM values are indicated. For example, SST (+4K) represents an increase in average global sea surface temperature of 4 K from the LGM to preindustrial era with a response of +0.5‰ and +30 ppm in $\delta^{13}C$(atm) and $[CO_2]$, respectively, as indicated by the respective black dots [*Köhler et al.*, 2010]. The sea ice coverage was reduced by 35% and 25% in the Northern and Southern Hemispheres, respectively. NADW and SO upwelling strength increased by 60% and 200%, respectively. Note that we are approximating the response of $\delta^{13}C$(atm) and $[CO_2]$ to each of these processes as linear.

of vegetation due to ice sheet expansion; and increase in sea ice in the Northern or Southern Hemisphere, leading to a reduction of uptake of isotopically heavy CO_2 by the ocean [*Köhler et al.*, 2010].

Figure 4 shows results of a modeling study [*Köhler et al.*, 2010] of the impacts of each of these processes on $[CO_2]$ and $\delta^{13}C$(atm). This plot illustrates that the first three mechanisms listed here are expected to lead to an increase in $\delta^{13}C$(atm) and a simultaneous decrease in $[CO_2]$, the reasons for which are discussed in more detail by *Köhler et al.* [2010].

In the case of scenarios 1 and 2, $\delta^{13}C$(ben) should show an overall decrease in this period as ^{13}C-depleted carbon is transferred from the surface to the deep ocean. However, the global benthic foraminiferal record does not show a decrease [*Raymo et al.*, 2004; *Oliver et al.*, 2010] but rather long-term variations superimposed on a rather constant $\delta^{13}C$(ben) level over MIS 5e-a. In fact, individual records from the North and South Atlantic [*Martínez-Méndez et al.*, 2009; *Charles et al.*, 2010] show—if any change—a slight increase in $\delta^{13}C$(ben) over the entire MIS 5, similar to $\delta^{13}C$(atm). The latter would point to a net exchange of a carbon from a reservoir outside of the atmosphere/ocean system being responsible for the observed carbon cycle changes, such as a net terrestrial carbon build up (process 3), probably related to peat buildup in this time of overall progressing glaciation. As illustrated in Figure 4, such a buildup in terrestrial biosphere also has the strongest impact on $\delta^{13}C$ in the atmosphere and ocean, while the sensitivity of $[CO_2]$ changes to this effect is the weakest per permille change in $\delta^{13}C$(atm). Accordingly, an increase in $\delta^{13}C$(atm) in this interval of 0.2–0.3‰ only implies a decrease in $[CO_2]$ of 10 ppm which is still within the possible long-term variation seen in $[CO_2]$ during this interval.

Previous studies have suggested that the reduction of sea ice during Termination I would lead to a decrease in $[CO_2]$ and $\delta^{13}C$(atm) [e.g., *Köhler et al.*, 2010], contrary to earlier studies where a large sea ice coverage is believed to be responsible for low atmospheric CO_2 concentrations [e.g., *Stephens and Keeling*, 2000]. Hence,

an expected growth of sea ice during Interval B could have also led to an increase in [CO_2] partly compensating a net transfer of carbon to the terrestrial biosphere while leading to a further increase in δ^{13}C(atm). Changes in sea surface temperature must have also played a role in driving carbon system changes during the early inception into the glacial. Based on the model results of *Köhler et al.* [2010], the cooling of the sea surface of 1–2 K in the high latitudes [*Schneider Mor et al.*, 2012; *Lawrence et al.*, 2009; *Köhler and Fischer*, 2006] could have led to a decrease in [CO_2] and δ^{13}C(atm) of up to 20 ppm and 0.2‰, respectively; however, this process would have again led to opposing effects in δ^{13}C in the atmosphere and the ocean.

In summary, based on the new data presented in this study, we are not able to quantitatively constrain the effects of all of these processes on [CO_2] and δ^{13}C(atm) without the use of our new data in dedicated modeling efforts. However, the concurrent change in δ^{13}C(atm) and δ^{13}C(ben) in the Atlantic suggests that a net growth of the terrestrial biosphere carbon storage (presumably by peat buildup) could have played a role.

4.2. Transient Changes at the Onset and End of MIS 4

Interval C (71.4–49.4 kyr B.P., see Figure 5) is characterized by the most pronounced variations in δ^{13}C(atm) during the last glacial and can be divided into seven subintervals defined by points at which the trend in [CO_2] changes. This division allows us to speculate which processes were most likely the major drivers of [CO_2] change during each of these periods; however, an unequivocal quantification of the size of the contribution of individual processes to the overall [CO_2] and δ^{13}C(atm) changes has to await future modeling studies.

I: For preindustrial conditions, the SO represents a "leak" of CO_2 to the atmosphere due to the upwelling of carbon- and nutrient-rich water from depths combined with a relatively inefficient marine biological soft-tissue pump defined by excess nutrients remaining in the surface ocean. This is in large part due to iron limitation. It has therefore been suggested [*Martin*, 1990] and confirmed by experiments [e.g., *Boyd et al.*, 2007] and models [e.g., *Hain et al.*, 2010] that significant increases in aeolian iron flux to the SO could cause a drawdown of CO_2 from the atmosphere into the ocean, thus reducing the oceanic CO_2 leakage, leading to a reduction in [CO_2] by up to 40 ppm. At the MIS 5-4 transition in Interval I, such an increase in Fe flux and corresponding decrease in [CO_2] has been documented, suggesting that this mechanism could play an important role at that time [e.g., *Martin*, 1990; *Martínez-Garcia et al.*, 2014; *Hain et al.*, 2010; *Jaccard et al.*, 2016]. However, our new data show that this cannot be the only mechanism at play, as the mean level of δ^{13}C(atm) does not change during Interval I. This time period is also marked by a decrease in temperature in Antarctica, represented here by the stable water isotopes δ^{18}O (EDML) and δD (EDC), which we also regard as representative of the phasing of temperature changes in the SO region. Fractionation of δ^{13}C(atm) across the air-water interface is temperature-dependent and decreases by approximately 0.1‰ per degree Celsius increase [*Mook et al.*, 1974; *Zhang et al.*, 1995; *Lynch-Stieglitz et al.*, 1995]. However, the sea surface temperatures (SST) of the SO and North Atlantic must be more heavily weighted with respect to carbon exchange with the ocean, as the surface waters in these regions are transported to depths through deepwater formation, thus efficiently transferring carbon and its associated isotopic signature to the ocean interior. Moreover, the isotopic fractionation is dependent on the degree of (isotopic) equilibrium reached during air/sea gas exchange before surface water is exported to the deep ocean. This equilibration is itself dependent on [CO_2] [*Galbraith et al.*, 2015] and may deviate somewhat from the value given above. However, in our interpretation we rely on the model-derived δ^{13}C(atm)/SST sensitivity derived by *Köhler et al.* [2010], which is very close to the value given above and should include such disequilibrium effects.

At the MIS 5-4 transition, the global average SST decreased by approximately 1°C [*Shakun et al.*, 2015], with a slightly more pronounced drop of about 2°C in the SO [*Crosta et al.*, 2004; *Schneider Mor et al.*, 2005; *Martínez-Garcia et al.*, 2009; *Ho et al.*, 2012]. Accordingly, this would have led to a decrease in δ^{13}C(atm) of 0.1–0.2‰, though the corresponding increase in sea ice in the high latitudes may have slightly compensated the decrease in both [CO_2] and δ^{13}C(atm). Thus, 0.2‰ is an upper limit of the effect of SST on δ^{13}C(atm) during this interval. As the δ^{13}C(atm) signal shows only a negligible change (at most an increase of approximately 0.05‰, which is within our experimental error), the influence of Fe fertilization could have caused at most a rise in δ^{13}C of 0.25‰ if it quantitatively counterbalanced the SST effect leading to the δ^{13}C(atm) signal observed during Interval I. Proxies for NADW production, including ϵ_{Nd} and ^{231}Pa/^{230}Th from marine cores in the North Atlantic, allow for a possible reduction in NADW during this period, although this change would have been small [*Böhm et al.*, 2014]. A decrease in NADW production is expected to have led to a small decrease in [CO_2] and increase in δ^{13}C; both of these changes are in the same direction as the effect of iron fertilization on atmospheric carbon. Thus, our estimate of Fe fertilization effects can be regarded as an upper

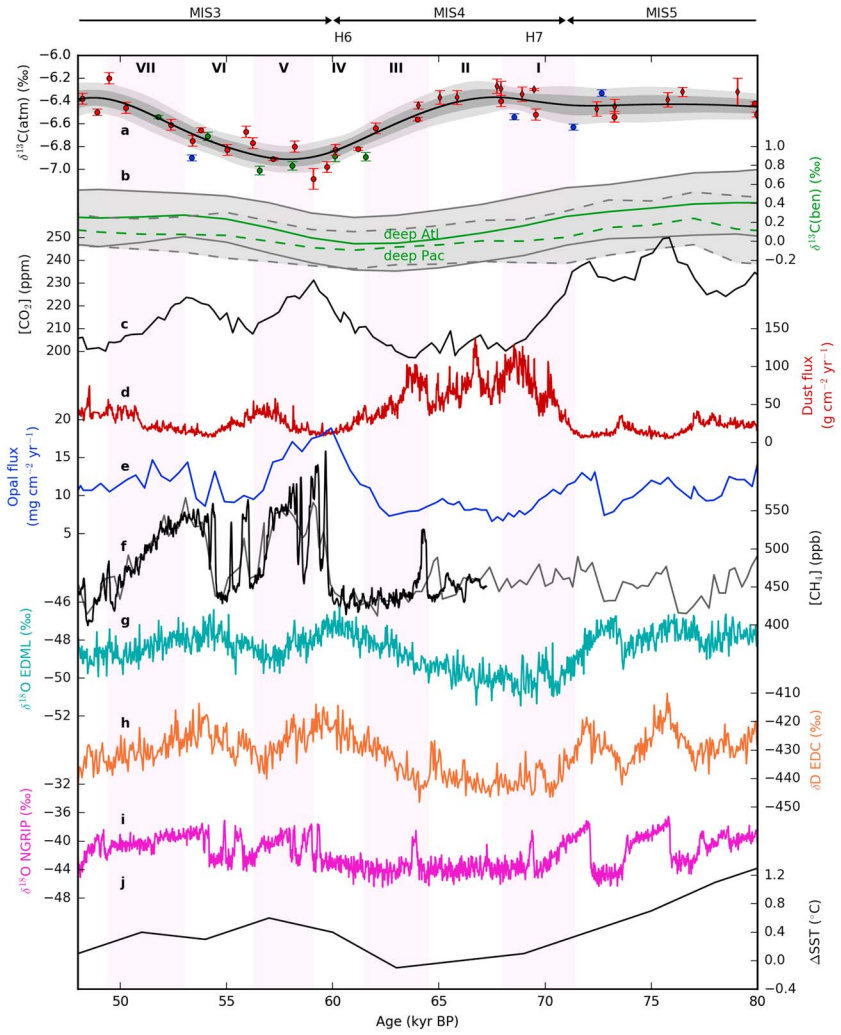

Figure 5. (a) δ^{13}C(atm) record in the time interval 80–48 kyr B.P. with other atmospheric and marine parameters. At the MIS 4-3 transition shown here, the new data show a pronounced drop followed by an equally large rise with an amplitude (approximately 0.5‰) similar to that observed at Termination I. (b) δ^{13}C(ben) values represent deep ocean (2500–5000 m) averages for the Atlantic and Pacific basins [*Oliver et al.*, 2010]. (c) [CO_2] (for sources see Figure 1) decreases and then increases rapidly at the onset and termination of MIS 4, respectively, and is thus not in phase with the significant decrease and subsequent increase in δ^{13}C(atm). (d) Dust flux at EDC [*Lambert et al.*, 2012]. (e) SO opal flux from core TN057-14PC (*Jaccard et al.* [2016] and *Anderson et al.* [2009], age scale as published). (f) [CH_4] at EDC (gray: *Loulergue et al.* [2008]) and WAIS (black: *Rhodes et al.* [2015] and *Buizert et al.* [2015]) show high-frequency fluctuations primarily due to wetland response. (g) EDML $\delta^{18}O(H_2O)$ [*EPICA Community Members*, 2006] and (h) EDC $\delta D(H_2O)$ [*Jouzel et al.*, 2007] are proxies for Antarctic temperature influenced by the bipolar seesaw process, which is controlled by rapid changes in the North Atlantic as documented in (i) NorthGRIP $\delta^{18}O(H_2O)$ [*NGRIP Community Members*, 2004]. (j) The stacked global average SST record compiled by (*Shakun et al.* [2015], age scale as published) is presented with respect to the LGM. Note that although the ice core data are synchronized using the AICC2012 timescale, some uncertainty is associated with the relative age scales of the ice cores and marine sediment cores.

bound on the possible effects of marine soft-tissue pump effects. The amplitude of these changes are roughly in line with corresponding estimates for the decline in [CO_2] of 10–20 ppm (SST) and ≈20 ppm (Fe fertilization) modeled by *Köhler et al.* [2010] for similar changes in proxy records at Termination I and are also in agreement with observations during selected AIM events during MIS 3 [*Schüpbach et al.*, 2013; *Röthlisberger et al.*, 2004].

II: In this interval, both the δ^{13}C and [CO_2] records show relatively small changes, suggesting that the global carbon system had reached a temporary equilibrium. It is important to note that the proposed increase in the soft-tissue pump efficiency in the surface SO during Interval I would have led to an increase in respired carbon at depths and thus an increase in deep ocean alkalinity. Over the course of the following millennia [e.g.,

Marchitto et al., 2005], carbonate compensation would have played an important role in redistributing the excess alkalinity, ultimately leading to further small and delayed changes in [CO_2] [*Sigman and Boyle*, 2000; *Hain et al.*, 2010]. This mechanism has only a very small impact on δ^{13}C(atm) [*Köhler et al.*, 2010; *Galbraith et al.*, 2015]. Please note that throughout the text we refer only to the direct immediate effect of synchronous environmental changes when discussing changes in the soft-tissue pump, while the delayed long-term readjustment of alkalinity connected to such a change is hard to discern in our data.

We regard it as likely that throughout Interval II, the input of aeolian dust to the SO surface ocean exceeded a threshold for Fe limitation of the marine biological soft-tissue pump in the SO. This hypothesis is corroborated by Fe and alkenone flux data from two neighboring marine sediment cores, TN057-6 and ODP 1090, in the eastern South Atlantic: these records show a simultaneous peak at the beginning of this interval and a subsequent decline from 68–61 kyr B.P. [*Sachs and Anderson*, 2003; *Martínez-Garcia et al.*, 2014]. Additionally, water isotopes from Antarctic ice cores indicate that temperatures in the SO region were fairly constant, indicating that no significant change in solubility or fractionation at the air-sea interface is expected to have influenced [CO_2] or δ^{13}C(atm) during this interval.

North Atlantic marine sediment core ϵ_{Nd} and ^{231}Pa/^{230}Th data indicate that this interval saw a weakening of the AMOC which lasted over the entire duration of MIS 4. This is evidenced by the relatively high values of ϵ_{Nd} at site ODP 1063 in the northwestern Atlantic on the Bermuda Rise (representative of the local presence of AABW) coupled to low ^{231}Pa/^{230}Th (indicating a combination of AABW and NADW in the water column above the core) [*Böhm et al.*, 2014]. Although the AMOC was certainly not in an "off" state at this time, as was the case during Heinrich events 2 and 1 [*Böhm et al.*, 2014], it is likely that the circulation pattern was in a "cold" state, in which deep water was formed in the North Atlantic but was not dense enough to sink to the bottom of the ocean basin and was underlain by AABW over larger parts of the Atlantic. The cooling that had occurred during Interval I in the Southern Hemisphere led to an expansion of sea ice around Antarctica; sea salt derived Na^+ flux data from ice cores suggest that the maximal extent of sea ice during the glacial may have been reached during the onset of MIS 4, persisting until the glacial termination [*Wolff et al.*, 2006; *Fischer et al.*, 2007], with substantial impacts on the carbon turnover in the deep ocean as well. Thus, the circulation pattern in the Atlantic may have more closely resembled two disconnected branches of deep water rather than the modern pattern, in which there is partial mixing of NADW and AABW [*Ferrari et al.*, 2014]. This would in turn have inhibited the release of isotopically light carbon from the deep SO that had already been sequestered during Interval I. These lines of evidence and the observation of constantly low [CO_2] and constant δ^{13}C(atm) in Interval II together imply that most of the net carbon transfer to the deep ocean was already completed during Interval I.

III: This period witnessed a major decrease in Fe flux and therefore probably also a reduction of the marine biological soft-tissue pump efficiency in the SO. As the Fe flux signal is roughly symmetrical at the beginning and end of MIS 4, we surmise that if Fe fertilization caused a 0.25‰ increase in δ^{13}C(atm) and approximately 20 ppm drop in [CO_2], at the beginning of MIS 4, the change due to the reduction in Fe flux at the end of MIS 4 would have caused changes of approximately the same magnitude but in the opposite direction. Thus, the effect of reduction of Fe flux to the SO largely occurred during Interval III, where the observed changes in both δ^{13}C(atm) and [CO_2] are in line with the respective estimates of changes in these parameters. Moreover, other proxy records show no significant changes during this interval (e.g., ϵ_{Nd}, δ^{13}C(ben), [CH_4], and opal flux). The rise in SST in the SO paired with cold conditions in the North Atlantic would have had opposite effects on changes in δ^{13}C(atm) and [CO_2], conceivably with a very small net global effect. This is also supported by small changes in SST and deep ocean temperature during and after MIS 4 as derived from marine sediment records [*Shakun et al.*, 2015].

IV: As evidenced by a peak in opal flux in the SO, the residual drop in δ^{13}C and rise in [CO_2] were likely due to an increase in SO upwelling that occurred after the major decline in Fe fertilization, releasing carbon from the deep ocean where it had been stored in the less well-ventilated ocean during MIS 4. This upwelling event appears to have occurred synchronously within the error limits with Heinrich event 6 in the North Atlantic. It is likely, however, that mixing did not fully increase to interglacial levels and that a southern sourced deep water mass with high concentrations of relatively δ^{13}C-depleted carbon remained present, as δ^{13}C(ben) begins to increase in this interval both in the deep Atlantic and Pacific but does not reach the interglacial level until after the glacial termination [*Oliver et al.*, 2010]. This reconfiguration of the deep water masses is in line with ϵ_{Nd} data from the northwestern Atlantic [*Böhm et al.*, 2014] as well as the hypothesis for delayed [CO_2] peaks

during AIM events in MIS 3 put forth by *Bereiter et al.* [2012]. An exchange of carbon from the ocean to the atmosphere is also supported considering the δ^{13}C(ben) increase during this interval, which is opposite to the decreasing trend in δ^{13}C(atm). This is similar to the upwelling event that occurred during Heinrich event 1 during the last glacial termination, which has independently been supported by oversaturation of dissolved CO_2 relative to the atmosphere both in the eastern equatorial Pacific and SO surface waters as expected from a net outgassing from the ocean rather than release from land [*Martínez-Botí et al.*, 2015].

The occurrence of Heinrich event 6 did not only have an influence on ocean circulation, but the effects of such events are recorded in chemical signals worldwide, including the Cariaco Basin [*Peterson et al.*, 2000], Hulu Cave in China [*Wang*, 2001], Arabian Sea [*Schulz et al.*, 1998], Santa Barbara Basin [*Behl and Kennett*, 1996], and the western Pacific Warm Pool [*Shiau et al.*, 2011], due to the global impact of the AMOC and related changes in the position of the intertropical convergence zone. Although some model results indicate that a weakening of the AMOC may have resulted in an increase in carbon storage in terrestrial vegetation [e.g., *Schmittner and Galbraith*, 2008; *Bouttes et al.*, 2012], others indicate that a decrease in these stocks is possible [e.g., *Menviel et al.*, 2008; *Bozbiyik et al.*, 2011].

V: The warming of the Northern Hemisphere that marked the beginning of MIS 3—as seen in the stable water isotope record from Greenland and associated with DO events 17 and 16—was likely associated with a slow regrowth of the terrestrial biosphere starting in this interval. This is evidenced by the stagnation in δ^{13}C(atm) and a small overall increase in deep sea δ^{13}C(ben) [*Oliver et al.*, 2010] along with a decrease in [CO_2]. The observed signals in atmospheric [CO_2] and δ^{13}C could also be explained by the decrease in SO upwelling during this interval, as evidenced by the drop in opal flux. Note that while SO upwelling enhances the transport of water containing relatively high concentrations of isotopically light carbon to the surface ocean, thus leading to an increase in [CO_2] and a decrease in δ^{13}C(atm) through air-sea gas exchange, this effect could be partly compensated by an increase in marine export production in the surface ocean due to an increase in the upwelling of nutrients; however, models show that the former effect dominates in magnitude [e.g., *Watson and Naveira Garabato*, 2006; *Hain et al.*, 2010].

The DO interstadials may have also been associated with a strengthening of the AMOC, but this would likely have led to an increase in [CO_2] and a decrease in δ^{13}C(atm) [*Köhler et al.*, 2010], not supported by our data. Also of note in this interval is a slight decrease in the SO SST (approximately 0.4°C) [*Köhler and Fischer*, 2006], which may have contributed to the reduction in [CO_2], simultaneously, however, causing a slight decrease in δ^{13}C(atm), providing a possible explanation for the stagnation in the signal of the latter. The effects of this cooling would have been partly compensated by a potential expanse of sea ice in the high southern latitudes, limiting gas exchange in the regions of deepwater formation.

VI: This interval is defined by a rise in both [CO_2] and δ^{13}C(atm). The lack of a similar upwelling signal in the SO (indicated by increasing [CO_2] and decreasing δ^{13}C(atm)) compared to Interval IV despite the occurrence of Heinrich event 5a at that time [*Rashid et al.*, 2003] suggests that the upwelling and release of old respired carbon into the atmosphere at this point was overcompensated by other processes. The increase in temperature in the Southern Hemisphere in this interval could help to explain the measurements, as an increase in SO SST would have led to an increase in both [CO_2] and δ^{13}C(atm) due to the decreased solubility and fractionation of CO_2 at higher temperatures. Interval VI may have also been associated with continued regrowth of vegetation on land, as suggested by a co-occurring shift in δ^{13}C(ben) and δ^{13}C(atm), while drawing down [CO_2] from the atmosphere. The cold temperatures recorded in Greenland as well as relatively enriched ϵ_{Nd} values in the northwestern Atlantic [*Böhm et al.*, 2014] indicate a weakened state of the AMOC, which is predicted to have had a similar effect on both parameters. The magnitudes of these processes must have been limited, however, as SST and deep ocean temperature changed little during MIS 3 [*Shakun et al.*, 2015], and the warming in the SO was not extraordinarily pronounced (≈0.3°C increase in SO SST predicted by *Köhler and Fischer* [2006], which would only produce a change in δ^{13}C(atm) within the uncertainty of the measurement).

VII: The last interval of this period, approximately concurrent with DO 14, is defined by the final stage of the clear increase in δ^{13}C(atm) coupled with a steep decline in [CO_2] but very little change in δ^{13}C(ben). Similar to what has been observed in the second half of Termination I [*Schmitt et al.*, 2012], a continued growth of the terrestrial biosphere could be expected, which would readily explain the δ^{13}C(atm) and [CO_2] changes in this interval. The lack of a clear δ^{13}C(ben) signal in the same direction in the global compilation by *Oliver et al.* [2010], which would be expected from terrestrial biosphere storage changes, questions this interpretation; however, individual δ^{13}C(ben) records [e.g., *Charles et al.*, 2010] show a much clearer increase in δ^{13}C(ben) at

that time. *Köhler and Fischer* [2006] also predict a small drop in SO SST, which would further have reduced $[CO_2]$ while leading to a depletion in $\delta^{13}C$(atm), contrary to what is observed.

4.3. $[CO_2]$ and $\delta^{13}C$(atm) Variability During MIS 3

Due in part to technical difficulties presented by samples in Interval D (49.4–18.7 kyr B.P.) (see "Data quality: Outliers" above), the data quality renders the discussion of millennial-scale variations in $\delta^{13}C$(atm) over this interval more difficult. However, certain features are still visible in the record. Overall $\delta^{13}C$(atm) is on a relatively stable level throughout MIS 3 which is close to value at the LGM; however, several longer-term negative fluctuations in $\delta^{13}C$(atm) appear to be supported by our data. Most importantly the data suggest two negative anomalies in $\delta^{13}C$(atm) which appear to be synchronous to the pronounced local $[CO_2]$ maxima in parallel to AIM 8 and 12, coupled as well with the dust flux to the SO (Figure 1). The latter is at a minimum at those times [e.g., *Martínez-Garcia et al.*, 2014], suggesting a re-emerging iron limitation of the marine soft-tissue pump for those intervals. In contrast, during the second half of MIS 3 the dust flux always exceeds the threshold for iron limitation and consequently the increased soft-tissue pump leads to rather high $\delta^{13}C$(atm) and low $[CO_2]$ while at the same time $\delta^{13}C$(ben) is at its lower limit. Note, however, that a concurrent increased stratification of the SO surface waters would also lead to an increase in the soft-tissue pump efficiency and cannot be discerned based on our records.

While the concurrent changes in dust flux provide a straightforward mechanistic understanding for a decreased soft-tissue pump during AIM 8 and 12, the ultimate reason for the climate changes in the SO and in their wake of carbon cycle changes comes about by the bipolar seesaw coupling with the North Atlantic. As shown in previous publications the AIM events are coupled to the DO events recorded in the Greenland record [*EPICA Community Members*, 2006; *Blunier and Brook*, 2001] via changes in the AMOC. Thereby the strongest increases in Antarctic temperature and $[CO_2]$ are not only observed during Heinrich events 4, 5, 5a, and 6 but also during Heinrich event 1 at the onset of the termination. Note that while Heinrich event 2 may also have left a small imprint in our $\delta^{13}C$(atm) record, an unambiguous signal of the weaker Heinrich event 3 cannot be discerned. However, the low resolution in the $\delta^{13}C$(atm) record at that time precludes a final conclusion.

Only recently, *Gottschalk et al.* [2015] showed that each MIS 3 stadial leaves a geochemical fingerprint in the Atlantic Ocean, although direct overturning proxies show only a clear signal for Heinrich events [*Böhm et al.*, 2014]. Changes in the AMOC are also connected to increased upwelling of nutrient-enriched and ^{13}C-depleted waters in the SO [*Anderson et al.*, 2009; *Sachs and Anderson*, 2005] most likely traceable to changes in the buoyancy flux due to accumulation of heat as a result of the bipolar seesaw [*Watson and Naveira Garabato*, 2006] or potentially also to a southward shift in the Southern Hemisphere westerlies [*Toggweiler et al.*, 2006]. In combination with increased iron limitation in the SO, this upwelling leads to outgassing of CO_2 from the SO surface ocean and, thus, the pronounced local $[CO_2]$ maxima and $\delta^{13}C$(atm) minima during those times. Future highly resolved records of $\delta^{13}C$(atm) during MIS 3, for example, from the West Antarctic Ice Sheet (WAIS) Divide ice core [*WAIS Divide Project Members*, 2015] will be able to further elucidate these millennial-scale events, thus adding significantly to our understanding of the role of ocean circulation and the global carbon cycle during MIS 3.

4.4. Comparison of the MIS 4-3 Transition and Termination I

Several climatic proxies show similarities in the records during MIS 4 and MIS 2, such as summer insolation in the Northern Hemisphere, the pronounced peaks in aeolian iron flux [*EPICA Community Members*, 2004; *Martínez-Garcia et al.*, 2009; *Lambert et al.*, 2012] and the extent of glaciers in New Zealand [*Schaefer et al.*, 2015]. Atmospheric $[CO_2]$ was reduced to $\approx$200 ppm during MIS 4, similar to that at the PGM and only approximately 10 ppm higher than $[CO_2]$ during the LGM. The transition into MIS 3 is similar in the $[CO_2]$ slope to the initial rise in $[CO_2]$ at Termination I (see Figures 5 and 6). However, at the MIS 4-3 transition, this increase was limited to approximately 30 ppm and $[CO_2]$ started to decrease again at around 59 kyr B.P.; the trend of rising temperatures in the Southern Hemisphere also reversed at this point, thus circumventing a transition to full interglacial conditions at this point. Perhaps unsurprisingly, the signal in our new $\delta^{13}C$(atm) data is also very similar at these two transitions; indeed, MIS 4-3 and Termination I mark the periods of the largest excursion in $\delta^{13}C$(atm) in the entire record of 0.4–0.5‰.

It is not yet clear what caused the end of the warming that began at MIS 4-3, which could be regarded as a "terminated termination," though theories have been proposed. *Wolff et al.* [2009] suggested that the timing of warming in the Northern Hemisphere (i.e., DO events) is the most important factor. Through the bipolar seesaw, the onset of a DO event leads to cooling in the Southern Hemisphere, thus preventing a complete

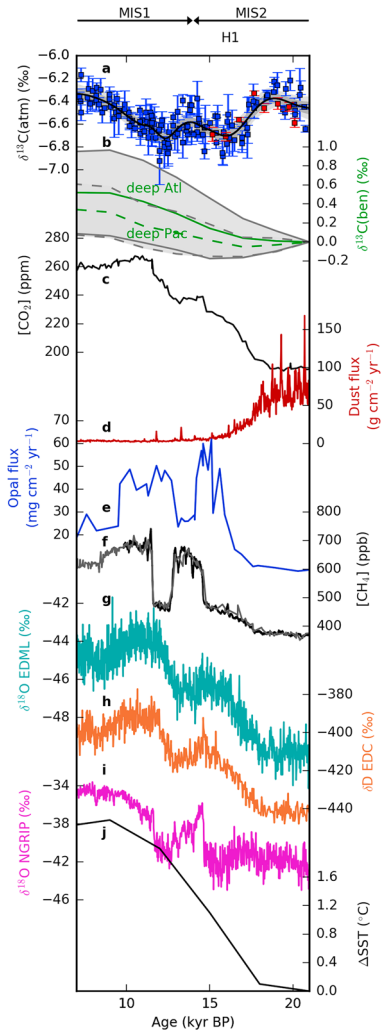

Figure 6. As in Figure 5 but for the late glacial maximum, Termination I, and the early Holocene. The amplitude of the δ^{13}C(atm) signal is similar to that at the MIS 4-3 transition, as is the slope in the initial [CO_2] rise. DO 1, seen as the abrupt increase in δ^{18}O in NGRIP, caused intermittent cooling in the Southern Hemisphere similar to event 17 at 63 kyr B.P. (Figure 5). However, DO 1 occurred only after [CO_2] had already risen by 60 ppm during Termination I, while the [CO_2] increase was only 30 ppm when DO 17 occurred.

glacial termination. *Schaefer et al.* [2015] proposed that the size of the Northern Hemisphere ice sheets is the determining factor for the initiation of a DO event, as these only reached 80% of their LGM volume in MIS 4 and were reduced to 50% of their maximum volume after the transition to MIS 3. The maximum size of the Northern Hemisphere ice sheets at the LGM may have suppressed the initiation of DO events [*Zhang et al.*, 2014] for an extended period and, thus, a bipolar seesaw response in the Southern Hemisphere in the first half of Termination I. The smaller ice sheet size during the MIS 4-3 transition, however, may have been below the threshold hypothesized by *Parrenin and Paillard* [2003] and others, thus allowing for occurrence of early DO events, which led to an uptake of CO_2 in the SO through the bipolar seesaw mechanism and halted the planetary warming, ultimately leading to a failed glacial/interglacial transition at that time [*Wolff et al.*, 2009].

While we cannot prove or disprove either of these theories with our new data alone, we can confirm that the lack of a glacial termination at 60 kyr B.P. was most likely not the result of significant differences between these periods in either the carbon stocks in the major reservoirs or the processes responsible for the major transfers of carbon among these reservoirs. As discussed above, the same mechanisms can be used to explain the signal observed in the δ^{13}C(atm) record at the MIS 4-3 transition as at Termination I, where the latter has been discussed in more detail by *Schmitt et al.* [2012]. To some extent, we can also confirm that the magnitudes of the changes in [CO_2] due to these processes were similar, for example, in the case of aeolian iron flux.

5. Conclusions

We have presented the first complete record of $\delta^{13}C(atm)$ over the last glacial/interglacial cycle. Small offsets exist between data from Talos Dome and EDML in $\delta^{13}C(atm)$ 47–43 kyr B.P. and in $[CO_2]$ 62–42 kyr B.P., which are difficult to explain by in situ production of CO_2 originating from organic or inorganic material in Talos Dome. The brittle zone in the ice core presents special technical difficulties due to the higher probability of sample contamination with drilling fluid; thus, measurements from a separate ice core from a region with a higher accumulation rate, such as the WAIS Divide ice core, could be instrumental in resolving these offsets as well as in filling the low-resolution "gap" in the current data set (35–22 kyr B.P.). The difference in accumulation rate would place the troublesome BCTZ at an earlier age in this record, and the period in question would be comprised solely of clathrate ice, which is less problematic with respect to drilling fluid intrusions.

Despite these technical issues, a large signal in $\delta^{13}C(atm)$ has been resolved in the interval 65–49 kyr B.P. The amplitude of this initial drop and the subsequent equally steep rise (approximately 0.5‰) is comparable to that seen at Termination I, indicating that similar processes were involved at the MIS 2-1 and MIS 4-3 transitions. Similar to Termination I, the large change in $\delta^{13}C(atm)$ is not synchronous with the carbon changes recorded by $\delta^{13}C(ben)$ in the deep ocean. As discussed in previous studies [e.g., *Köhler et al.*, 2010; *Schmitt et al.*, 2012; *Schneider et al.*, 2013], these processes most likely included a combination of changes in SST, the terrestrial biosphere, AMOC strength, SO stratification and upwelling, and the efficiency of the marine biological soft-tissue pump.

Of note is the fact that iron fertilization (10–20 ppm in $[CO_2]$) cannot be the only process to explain our observations at the MIS 5-4 transition deduced from the timing and amplitude of the $\delta^{13}C(atm)$ signal. While $[CO_2]$ drops significantly at this transition, the stable carbon isotope responds only minimally, indicating that the increased efficiency of marine export, transferring ^{13}C-depleted carbon from the surface ocean to depths and consequently raising $\delta^{13}C$ in the surface ocean and atmosphere, must have been approximately balanced by the effect of decreasing SST, thus constraining the total effect of Fe fertilization on $\Delta[CO_2]$ and $\Delta\delta^{13}C(atm)$. By arguing that the impact of Fe fertilization on these two parameters must have been similar in magnitude but opposite in direction at the MIS 5-4 and MIS 4-3 transitions, we further assert that the $[CO_2]$ rise during the latter was only in part caused by a reduction of marine biological export to depths; it is likely that approximately half the signal should be ascribed to an increase in SO upwelling. This in turn indicates that the ocean must have been more stratified during MIS 4, allowing for the storage of light inorganic carbon at depths, some of which was released at the MIS 4-3 transition. Thus, we concur with previous studies [*Bereiter et al.*, 2012; *Adkins*, 2013; *Jaccard et al.*, 2016], which have suggested it to be it is likely that a transfer of light carbon to ocean depths intensified at the MIS 5-4 transition.

Acknowledgments
The data of this study are available electronically at the PANGAEA® Data Publisher for Earth and Environmental Science (URL: http://www.pangaea.de). The authors would like to thank Gregory Teste and Jérôme Chappellaz for their generous donation of time and ice samples from the EDML ice core as well as Peter Köhler for the BICYCLE model results presented here. We are additionally indebted to Daniel Baggenstos, Thomas Bauska, Ed Brook, Juerg Schaefer, Todd Sowers, and Eric Galbraith for their fruitful discussion. Financial support for this work was provided by the Swiss National Science Foundation. This is EPICA publication no. 304 and TALDICE publication no. 43.

References

Adkins, J. F. (2013), The role of deep ocean circulation in setting glacial climates, *Paleoceanography*, *28*(3), 539–561, doi:10.1002/palo.20046.

Ahn, J., and E. J. Brook (2008), Atmospheric CO_2 and climate on millennial time scales during the last glacial period, *Science*, *322*(5898), 83–85, doi:10.1126/science.1160832.

Ahn, J., E. J. Brook, and C. Buizert (2014), Response of atmospheric CO_2 to the abrupt cooling event 8200 years ago, *Geophys. Res. Lett.*, *41*(2), 604–609, doi:10.1002/2013gl058177.

Anderson, R. F., S. Ali, L. I. Bradtmiller, S. H. H. Nielsen, M. Q. Fleisher, B. E. Anderson, and L. H. Burckle (2009), Wind-driven upwelling in the Southern Ocean and the deglacial rise in atmospheric CO_2, *Science*, *323*(5920), 1443–1448, doi:10.1126/science.1167441.

Anderson, R. F., S. Barker, M. Fleisher, R. Gersonde, S. L. Goldstein, G. Kuhn, P. G. Mortyn, K. Pahnke, and J. P. Sachs (2014), Biological response to millennial variability of dust and nutrient supply in the Subantarctic South Atlantic Ocean, *Philos. Trans. R. Soc. A*, *372*(2019), 20130054, doi:10.1098/rsta.2013.0054.

Barker, S., J. Chen, X. Gong, L. Jonkers, G. Knorr, and D. Thornalley (2015), Icebergs not the trigger for North Atlantic cold events, *Nature*, *520*(7547), 333–336, doi:10.1038/nature14330.

Baumgartner, M., et al. (2014), NGRIP CH_4 concentration from 120 to 10 kyr before present and its relation to a $\delta^{15}N$ temperature reconstruction from the same ice core, *Clim. Past*, *10*(2), 903–920, doi:10.5194/cp-10-903-2014.

Bazin, L., et al. (2013), An optimized multi-proxy, multi-site Antarctic ice and gas orbital chronology (AICC2012): 120–800 ka, *Clim. Past*, *9*(4), 1715–1731, doi:10.5194/cp-9-1715-2013.

Behl, R. J., and J. P. Kennett (1996), Brief interstadial events in the Santa Barbara basin, NE Pacific, during the past 60 kyr, *Nature*, *379*(6562), 243–246, doi:10.1038/379243a0.

Bereiter, B., J. Schwander, D. Lüthi, and T. F. Stocker (2009), Change in CO_2 concentration and O_2/N_2 ratio in ice cores due to molecular diffusion, *Geophys. Res. Lett.*, *36*(5), doi:10.1029/2008GL036737.

Bereiter, B., D. Lüthi, M. Siegrist, S. Schüpbach, T. F. Stocker, and H. Fischer (2012), Mode change of millennial CO_2 variability during the last glacial cycle associated with a bipolar marine carbon seesaw, *Proc. Natl. Acad. Sci.*, *109*(25), 9755–9760, doi:10.1073/pnas.1204069109.

Blunier, T., and E. J. Brook (2001), Timing of millennial-scale climate change in Antarctica and Greenland during the last glacial period, *Science*, *291*(5501), 109–112, doi:10.1126/science.291.5501.109.

Böhm, E., J. Lippold, M. Gutjahr, M. Frank, P. Blaser, B. Antz, J. Fohlmeister, N. Frank, M. B. Andersen, and M. Deininger (2014), Strong and deep Atlantic meridional overturning circulation during the last glacial cycle, *Nature*, *517*(7532), 73–76, doi:10.1038/nature14059.

Bouttes, N., D. M. Roche, and D. Paillard (2012), Systematic study of the impact of fresh water fluxes on the glacial carbon cycle, *Clim. Past*, *8*(2), 589–607, doi:10.5194/cp-8-589-2012.

Boyd, P. W., et al. (2007), Mesoscale iron enrichment experiments 1993–2005: Synthesis and future directions, *Science*, *315*(5812), 612–617, doi:10.1126/science.1131669.

Bozbiyik, A., M. Steinacher, F. Joos, T. F. Stocker, and L. Menviel (2011), Fingerprints of changes in the terrestrial carbon cycle in response to large reorganizations in ocean circulation, *Clim. Past*, *7*(1), 319–338, doi:10.5194/cp-7-319-2011.

Broecker, W. S. (1998), Paleocean circulation during the last deglaciation: A bipolar seesaw?, *Paleoceanography*, *13*(2), 119–121, doi:10.1029/97PA03707.

Buiron, D., et al. (2011), TALDICE-1 age scale of the Talos Dome deep ice core, East Antarctica, *Clim. Past*, *7*(1), 1–16, doi:10.5194/cp-7-1-2011.

Buizert, C., et al. (2015), The WAIS Divide deep ice core WD2014 chronology—Part 1: Methane synchronization (68–31 ka BP) and the gas age-ice age difference, *Clim. Past*, *11*(2), 153–173, doi:10.5194/cp-11-153-2015.

Charles, C. D., K. Pahnke, R. Zahn, P. G. Mortyn, U. Ninnemann, and D. A. Hodell (2010), Millennial scale evolution of the Southern Ocean chemical divide, *Quat. Sci. Rev.*, *29*(3–4), 399–409, doi:10.1016/j.quascirev.2009.09.021.

Craig, H., Y. Horibe, and T. Sowers (1988), Gravitational separation of gases and isotopes in polar ice caps, *Science*, *242*, 1675–1678.

Crosta, X., A. Sturm, L. Armand, and J.-J. Pichon (2004), Late Quaternary sea ice history in the Indian sector of the Southern Ocean as recorded by diatom assemblages, *Mar. Micropaleontol.*, *50*(3–4), 209–223, doi:10.1016/s0377-8398(03)00072-0.

Elsig, J., J. Schmitt, D. Leuenberger, R. Schneider, M. Eyer, M. Leuenberger, F. Joos, H. Fischer, and T. F. Stocker (2009), Stable isotope constraints on Holocene carbon cycle changes from an Antarctic ice core, *Nature*, *461*(7263), 507–510, doi:10.1038/nature08393.

EPICA Community Members (2004), Eight glacial cycles from an Antarctic ice core, *Nature*, *429*, 623–628.

EPICA Community Members (2006), One-to-one coupling of glacial climate variability in Greenland and Antarctica, *Nature*, *444*(7116), 195–198, doi:10.1038/nature05301.

Ferrari, R., M. F. Jansen, J. F. Adkins, A. Burke, A. L. Stewart, and A. F. Thompson (2014), Antarctic sea ice control on ocean circulation in present and glacial climates, *Proc. Natl. Acad. Sci.*, *111*(24), 8753–8758, doi:10.1073/pnas.1323922111.

Fischer, H., M.-L. Siggaard-Andersen, U. Ruth, R. Röthlisberger, and E. Wolff (2007), Glacial/interglacial changes in mineral dust and sea-salt records in polar ice cores: Sources, transport, and deposition, *Rev. Geophys.*, *45*(1), RG1002, doi:10.1029/2005RG000192.

François, R., M. A. Altabet, E.-F. Yu, D. M. Sigman, M. P. Bacon, M. Frank, G. Bohrmann, G. Bareille, and L. D. Labeyrie (1997), Contribution of Southern Ocean surface-water stratification to low atmospheric CO_2 concentrations during the last glacial period, *Nature*, *389*(6654), 929–935, doi:10.1038/40073.

Galbraith, E. D., E. Y. Kwon, D. Bianchi, M. P. Hain, and J. L. Sarmiento (2015), The impact of atmospheric pCO_2 on carbon isotope ratios of the atmosphere and ocean, *Global Biogeochem. Cycles*, *29*(3), 307–324, doi:10.1002/2014gb004929.

Gottschalk, J., L. C. Skinner, and C. Waelbroeck (2015), Contribution of seasonal sub-Antarctic surface water variability to millennial-scale changes in atmospheric CO_2 over the last deglaciation and Marine Isotope Stage 3, *Earth Planet. Sci. Lett.*, *411*, 87–99, doi:10.1016/j.epsl.2014.11.051.

Hain, M. P., D. M. Sigman, and G. H. Haug (2010), Carbon dioxide effects of Antarctic stratification, North Atlantic Intermediate Water formation, and subantarctic nutrient drawdown during the last ice age: Diagnosis and synthesis in a geochemical box model, *Global Biogeochem. Cycles*, *24*(4), GB4023, doi:10.1029/2010GB003790.

Hemming, S. R. (2004), Heinrich events: Massive late Pleistocene detritus layers of the North Atlantic and their global climate imprint, *Rev. Geophys.*, *42*(1), RG1005, doi:10.1029/2003RG000128.

Ho, S. L., G. Mollenhauer, F. Lamy, A. Martínez-Garcia, M. Mohtadi, R. Gersonde, D. Hebbeln, S. Nunez-Ricardo, A. Rosell-Melé, and R. Tiedemann (2012), Sea surface temperature variability in the Pacific sector of the Southern Ocean over the past 700 kyr, *Paleoceanography*, *27*(4), doi:10.1029/2012PA002317.

Ikeda-Fukazawa, T., K. Fukumizu, K. Kawamura, S. Aoki, T. Nakazawa, and T. Hondoh (2005), Effects of molecular diffusion on trapped gas composition in polar ice cores, *Earth Planet. Sci. Lett.*, *229*(3–4), 183–192, doi:10.1016/j.epsl.2004.11.011.

Jaccard, S. L., C. T. Hayes, A. Martínez-Garcia, D. A. Hodell, R. F. Anderson, D. M. Sigman, and G. H. Haug (2013), Two modes of change in Southern Ocean productivity over the past million years, *Science*, *339*(6126), 1419–1423, doi:10.1126/science.1227545.

Jaccard, S. L., E. D. Galbraith, A. Martínez-García, and R. F. Anderson (2016), Covariation of deep Southern Ocean oxygeoxygen and atmospheric CO_2 through the last ice age, *Nature*, *530*, 207–210, doi:10.1038/nature16514.

Jouzel, J., et al. (2007), Orbital and millennial Antarctic climate variability over the past 800,000 years, *Science*, *317*(5839), 793–796, doi:10.1126/science.1141038.

Köhler, P., and H. Fischer (2006), Simulating low frequency changes in atmospheric CO_2 during the last 740,000 years, *Clim. Past*, *2*(2), 57–78, doi:10.5194/cp-2-57-2006.

Köhler, P., H. Fischer, and J. Schmitt (2010), Atmospheric $\delta^{13}CO_2$ and its relation to pCO_2 and deep ocean $\delta^{13}C$ during the late Pleistocene, *Paleoceanography*, *25*(1), doi:10.1029/2008PA001703.

Lambert, F., M. Bigler, J. P. Steffensen, M. Hutterli, and H. Fischer (2012), Centennial mineral dust variability in high-resolution ice core data from dome c, Antarctica, *Clim. Past*, *8*(2), 609–623, doi:10.5194/cp-8-609-2012.

Lawrence, K. T., T. D. Herbert, C. M. Brown, M. E. Raymo, and A. M. Haywood (2009), High-amplitude variations in North Atlantic sea surface temperature during the early Pliocene warm period, *Paleoceanography*, *24*(2), doi:10.1029/2008PA001669.

Lippold, J., J. Grützner, D. Winter, Y. Lahaye, A. Mangini, and M. Christl (2009), Does sedimentary $^{231}Pa/^{230}Th$ from the Bermuda Rise monitor past Atlantic Meridional Overturning Circulation?, *Geophys. Res. Lett.*, *36*(12), L12601, doi:10.1029/2009GL038068.

Loulergue, L., A. Schilt, R. Spahni, V. Masson-Delmotte, T. Blunier, B. Lemieux, J.-M. Barnola, D. Raynaud, T. F. Stocker, and J. Chappellaz (2008), Orbital and millennial-scale features of atmospheric ch4 over the past 800,000 years, *Nature*, *453*(7193), 383–386, doi:10.1038/nature06950.

Lourantou, A., J. Chappellaz, J.-M. Barnola, V. Masson-Delmotte, and D. Raynaud (2010a), Changes in atmospheric CO_2 and its carbon isotopic ratio during the penultimate deglaciation, *Quat. Sci. Rev.*, *29*(17–18), 1983–1992, doi:10.1016/j.quascirev.2010.05.002.

Lourantou, A., J. V.Lavrič, P. Köhler, J.-M. Barnola, D. Paillard, E. Michel, D. Raynaud, and J. Chappellaz (2010b), Constraint of the CO_2 rise by new atmospheric carbon isotopic measurements during the last deglaciation, *Global Biogeochem. Cycles*, *24*(2), GB2015, doi:10.1029/2009GB003545.

Lüthi, D., et al. (2008), High-resolution carbon dioxide concentration record 650,000–800,000 years before present, *Nature*, *453*(7193), 379–382, doi:10.1038/nature06949.

Lüthi, D., et al. (2010), CO_2 and O_2/N_2 variations in and just below the bubble-clathrate transformation zone of Antarctic ice cores, *Earth Planet. Sci. Lett.*, *297*(1–2), 226–233, doi:10.1016/j.epsl.2010.06.023.

Lynch-Stieglitz, J., T. F. Stocker, W. S. Broecker, and R. G. Fairbanks (1995), The influence of air-sea exchange on the isotopic composition of oceanic carbon: Observations and modeling, *Global Biogeochem. Cycles*, *9*(4), 653–665, doi:10.1029/95GB02574.
Marchitto, T. M., J. Lynch-Stieglitz, and S. R. Hemming (2005), Deep Pacific $CaCO_3$ compensation and glacial-interglacial atmospheric CO_2, *Earth Planet. Sci. Lett.*, *231*(3–4), 317–336, doi:10.1016/j.epsl.2004.12.024.
Marcott, S. A., et al. (2011), Ice-shelf collapse from subsurface warming as a trigger for Heinrich events, *Proc. Natl. Acad. Sci.*, *108*(33), 13,415–13,419, doi:10.1073/pnas.1104772108.
Martin, J. H. (1990), Glacial-interglacial CO_2 change: The iron hypothesis, *Paleoceanography*, *5*(1), 1–13, doi:10.1029/pa005i001p00001.
Martínez-Botí, M. A., G. Marino, G. L. Foster, P. Ziveri, M. J. Henehan, J. W. B.Rae, P. G. Mortyn, and D. Vance (2015), Boron isotope evidence for oceanic carbon dioxide leakage during the last deglaciation, *Nature*, *518*(7538), 219–222, doi:10.1038/nature14155.
Martínez-Garcia, A., A. Rosell-Melé, W. Geibert, R. Gersonde, P. Masqué, V. Gaspari, and C. Barbante (2009), Links between iron supply, marine productivity, sea surface temperature, and CO_2 over the last 1.1 Ma, *Paleoceanography*, *24*(1), doi:10.1029/2008PA001657.
Martínez-Garcia, A., D. M. Sigman, H. Ren, R. F. Anderson, M. Straub, D. A. Hodell, S. L. Jaccard, T. I. Eglinton, and G. H. Haug (2014), Iron fertilization of the subantarctic ocean during the last ice age, *Science*, *343*(6177), 1347–1350, doi:10.1126/science.1246848.
Martínez-Méndez, G., E. G. Molyneux, I. R. Hall, and R. Zahn (2009), Variable water column structure of the South Atlantic on glacial-interglacial time scales, *Quat. Sci. Rev.*, *28*(27–28), 3379–3387, doi:10.1016/j.quascirev.2009.09.022.
McManus, J. F., R. François, J.-M. Gherardi, L. D. Keigwin, and S. Brown-Leger (2004), Collapse and rapid resumption of Atlantic meridional circulation linked to deglacial climate changes, *Nature*, *428*, 834–837.
Menviel, L., A. Timmermann, A. Mouchet, and O. Timm (2008), Meridional reorganizations of marine and terrestrial productivity during Heinrich events, *Paleoceanography*, *23*(1), doi:10.1029/2007PA001445.
Menviel, L., F. Joos, and S. Ritz (2012), Simulating atmospheric CO_2, ^{13}C and the marine carbon cycle during the Last Glacial-Interglacial cycle: possible role for a deepening of the mean remineralization depth and an increase in the oceanic nutrient inventory, *Quat. Sci. Rev.*, *56*, 46–68, doi:10.1016/j.quascirev.2012.09.012.
Monnin, E., A. Indermühle, A. Dällenbach, J. Flückiger, B. Stauffer, T. F. Stocker, D. Raynaud, and J.-M. Barnola (2001), Atmospheric CO_2 concentrations over the last glacial termination, *Science*, *291*(5501), 112–114, doi:10.1126/science.291.5501.112.
Monnin, E., et al. (2004), Evidence for substantial accumulation rate variability in Antarctica during the Holocene, through synchronization of CO_2 in the Taylor Dome, Dome C and DML ice cores, *Earth and Planetary Science Letters*, *224*(1–2), 45–54, doi:10.1016/j.epsl.2004.05.007.
Mook, W. G., J. C. Bommerson, and W. H. Staverman (1974), Carbon isotope fractionation between dissolved bicarbonate and gaseous carbon dioxide, *Earth Planet. Sci. Lett.*, *22*(2), 169–176, doi:10.1016/0012-821x(74)90078-8.
Neff, P. D. (2014), A review of the brittle ice zone in polar ice cores, *Ann. Glaciol.*, *55*(68), 72–82, doi:10.3189/2014aog68a023.
NGRIP Community Members (2004), High-resolution record of Northern Hemisphere climate extending into the last interglacial period, *Nature*, *431*(7005), 147–151, doi:10.1038/nature02805.
Oliver, K. I. C., B. A. A. Hoogakker, S. Crowhurst, G. M. Henderson, R. E. M. Rickaby, N. R. Edwards, and H. Elderfield (2010), A synthesis of marine sediment core $\delta^{13}C$ data over the last 150,000 years, *Clim. Past*, *6*(5), 645–673, doi:10.5194/cp-6-645-2010.
Parrenin, F., and D. Paillard (2003), Amplitude and phase of glacial cycles from a conceptual model, *Earth Planet. Sci. Lett.*, *214*, 243–250.
Peterson, L. C., G. H. Haug, K. A. Hughen, and U. Röhl (2000), Rapid changes in the hydrologic cycle of the tropical Atlantic during the last glacial, *Science*, *290*(5498), 1947–1951, doi:10.1126/science.290.5498.1947.
Rashid, H., R. Hesse, and D. J. W. Piper (2003), Evidence for an additional Heinrich event between H5 and H6 in the Labrador Sea, *Paleoceanography*, *18*(4), 1077, doi:10.1029/2003PA000913.
Raymo, M. E., D. W. Oppo, B. P. Flower, D. A. Hodell, J. F. McManus, K. A. Venz, K. F. Kleiven, and K. McIntyre (2004), Stability of North Atlantic water masses in face of pronounced climate variability during the Pleistocene, *Paleoceanography*, *19*(2), PA2008, doi:10.1029/2003PA000921.
Rhodes, R. H., E. J. Brook, J. C. H. Chiang, T. Blunier, O. J. Maselli, J. R. McConnell, D. Romanini, and J. P. Severinghaus (2015), Enhanced tropical methane production in response to iceberg discharge in the North Atlantic, *Science*, *348*(6238), 1016–1019, doi:10.1126/science.1262005.
Roberts, N. L., A. M. Piotrowski, J. F. McManus, and L. D. Keigwin (2010), Synchronous deglacial overturning and water mass source changes, *Science*, *327*(5961), 75–78, doi:10.1126/science.1178068.
Röthlisberger, R., M. Bigler, E. W. Wolff, F. Joos, E. Monnin, and M. A. Hutterli (2004), Ice core evidence for the extent of past atmospheric CO_2 change due to iron fertilisation, *Geophys. Res. Lett.*, *31*(16), L16207, doi:10.1029/2004GB020338.
Sachs, J. P., and R. F. Anderson (2003), Fidelity of alkenone paleotemperatures in southern Cape Basin sediment drifts, *Paleoceanography*, *18*(4), 1082, doi:10.1029/2002PA000862.
Sachs, J. P., and R. F. Anderson (2005), Increased productivity in the subantarctic ocean during Heinrich events, *Nature*, *434*(7037), 1118–1121, doi:10.1038/nature03544.
Schaefer, J. M., et al. (2015), The Southern Glacial Maximum 65,000 years ago and its unfinished termination, *Quat. Sci. Rev.*, *114*, 52–60, doi:10.1016/j.quascirev.2015.02.009.
Schilt, A., et al. (2010), Atmospheric nitrous oxide during the last 140,000 years, *Earth and Planetary Science Letters*, *300*(1–2), 33–43, doi:10.1016/j.epsl.2010.09.027.
Schmitt, J., R. Schneider, and H. Fischer (2011), A sublimation technique for high-precision measurements of $\delta^{13}CO_2$ and mixing ratios of CO_2 and N_2O from air trapped in ice cores, *Atmos. Meas. Tech.*, *4*(7), 1445–1461, doi:10.5194/amt-4-1445-2011.
Schmitt, J., et al. (2012), Carbon isotope constraints on the deglacial CO_2 rise from ice cores, *Science*, *336*(6082), 711–714, doi:10.1126/science.1217161.
Schmittner, A., and E. D. Galbraith (2008), Glacial greenhouse-gas fluctuations controlled by ocean circulation changes, *Nature*, *456*(7220), 373–376, doi:10.1038/nature07531.
Schneider, R. (2011), Quantifying past changes of the global carbon cycle based on $\delta^{13}CO_2$ measurements in Antarctic ice cores, PhD thesis, Univ. of Bern, Switzerland.
Schneider, R., J. Schmitt, P. Köhler, F. Joos, and H. Fischer (2013), A reconstruction of atmospheric carbon dioxide and its stable carbon isotopic composition from the penultimate glacial maximum to the last glacial inception, *Clim. Past*, *9*(6), 2507–2523, doi:10.5194/cp-9-2507-2013.
Schneider Mor, A., R. Yam, C. Bianchi, M. Kunz-Pirrung, R. Gersonde, and A. Shemesh (2005), Diatom stable isotopes, sea ice presence and sea surface temperature records of the past 640 ka in the Atlantic sector of the Southern Ocean, *Geophys. Res. Lett.*, *32*(10), L10704, doi:10.1029/2005GL022543.
Schneider Mor, A., R. Yam, C. Bianchi, M. Kunz-Pirrung, R. Gersonde, and A. Shemesh (2012), Variable sequence of events during the past seven terminations in two deep-sea cores from the Southern Ocean, *Quat. Res.*, *77*(2), 317–325, doi:10.1016/j.yqres.2011.11.006.

Schulz, H., U. von Rad, and H. Erlenkeuser (1998), Correlation between Arabian Sea and Greenland climate oscillations of the past 110,000 years, *Nature*, *392*(6679), 847–847, doi:10.1038/31750.
Schüpbach, S., U. Federer, P. R. Kaufmann, S. Albani, C. Barbante, T. F. Stocker, and H. Fischer (2013), High-resolution mineral dust and sea ice proxy records from the Talos Dome ice core, *Clim. Past*, *9*(6), 2789–2807, doi:10.5194/cp-9-2789-2013.
Severinghaus, J. P., R. Beaudette, M. A. Headly, K. Taylor, and E. J. Brook (2009), Oxygen-18 of O_2 records the impact of abrupt climate change on the terrestrial biosphere, *Science*, *324*(5933), 1431–1434, doi:10.1126/science.1169473.
Shakun, J. D., D. W. Lea, L. E. Lisiecki, and M. E. Raymo (2015), An 800-kyr record of global surface ocean $\delta^{18}O$ and implications for ice volume-temperature coupling, *Earth Planet. Sci. Lett.*, *426*, 58–68, doi:10.1016/j.epsl.2015.05.042.
Shiau, L.-J., M.-T. Chen, S. C. Clemens, C.-A. Huh, M. Yamamoto, and Y. Yokoyama (2011), Warm pool hydrological and terrestrial variability near southern Papua New Guinea over the past 50k, *Geophys. Res. Lett.*, *38*(8), L00F01, doi:10.1029/2010GL045309.
Siegenthaler, U., et al. (2005), Stable carbon cycle-climate relationship during the late Pleistocene, *Science*, *310*(5752), 1313–1317, doi:10.1126/science.1120130.
Sigman, D. M., and E. A. Boyle (2000), Glacial/interglacial variations in atmospheric carbon dioxide, *Nature*, *407*(6806), 859–869, doi:10.1038/35038000.
Skinner, L. C., S. Fallon, C. Waelbroeck, E. Michel, and S. Barker (2010), Ventilation of the deep Southern Ocean and deglacial CO_2 rise, *Science*, *328*(5982), 1147–1151, doi:10.1126/science.1183627.
Stenni, B., et al. (2011), Expression of the bipolar see-saw in Antarctic climate records during the last deglaciation, *Nat. Geosci.*, *4*(1), 46–49, doi:10.1038/ngeo1026.
Stephens, B. B., and R. F. Keeling (2000), The influence of Antarctic sea ice on glacial-interglacial CO_2 variations, *Nature*, *404*(6774), 171–174, doi:10.1038/35004556.
Stocker, T. F. (1998), Climate change: The seesaw effect, *Science*, *282*(5386), 61–62, doi:10.1126/science.282.5386.61.
Stocker, T. F., and S. J. Johnsen (2003), A minimum thermodynamic model for the bipolar seesaw, *Paleoceanography*, *18*(4), 1087, doi:10.1029/2003PA000920.
Toggweiler, J. R., J. L. Russell, and S. R. Carson (2006), Midlatitude westerlies, atmospheric CO_2, and climate change during the ice ages, *Paleoceanography*, *21*(2), doi:10.1029/2005PA001154.
Tschumi, J., and B. Stauffer (2000), Reconstructing past atmospheric CO_2 concentration based on ice-core analyses: Open questions due to in situ production of CO_2 in the ice, *J. Glaciol.*, *46*(152), 45–53, doi:10.3189/172756500781833359.
Veres, D., et al. (2013), The Antarctic ice core chronology (AICC2012): An optimized multi-parameter and multi-site dating approach for the last 120 thousand years, *Clim. Past*, *9*(4), 1733–1748, doi:10.5194/cp-9-1733-2013.
WAIS Divide Project Members (2015), Precise interpolar phasing of abrupt climate change during the last ice age, *Nature*, *520*(7549), 661–665, doi:10.1038/nature14401.
Wang, Y. J. (2001), A high-resolution absolute-dated late Pleistocene monsoon record from Hulu Cave, China, *Science*, *294*(5550), 2345–2348, doi:10.1126/science.1064618.
Watson, A. J., and A. C. Naveira Garabato (2006), The role of Southern Ocean mixing and upwelling in glacial-interglacial atmospheric CO_2 change, *Tellus*, *58*(1), 73–87, doi:10.1111/j.1600-0889.2005.00167.x.
Wolff, E. W., et al. (2006), Southern Ocean sea-ice extent, productivity and iron flux over the past eight glacial cycles, *Nature*, *440*(7083), 491–496, doi:10.1038/nature04614.
Wolff, E. W., H. Fischer, and R. Röthlisberger (2009), Glacial terminations as southern warmings without northern control, *Nat. Geosci.*, *2*(3), 206–209, doi:10.1038/ngeo442.
Zhang, J., P. Quay, and D. Wilbur (1995), Carbon isotope fractionation during gas-water exchange and dissolution of CO_2, *Geochim. Cosmochim. Acta*, *59*(1), 107–114, doi:10.1016/0016-7037(95)91550-d.
Zhang, X., G. Lohmann, G. Knorr, and C. Purcell (2014), Abrupt glacial climate shifts controlled by ice sheet changes, *Nature*, *512*(7514), 290–294, doi:10.1038/nature13592.